「分光エリプソメトリによる半導体物性の研究」

Chapter 1

Introduction

1.1 Background

Ellipsometry is an optical technique for the characterization of and observation of events at an interface or film between two media and is based on exploiting the polarization transformation that occurs as a beam of polarized light is reflected from or transmitted through the interface or film. Its history dates back to the 19th century[1], but in the last ten years spectroscopic ellipsometry (SE), combined with the availability of microcomputers for both instrumental control and real-time analysis of results, has produced a renaissance in the technique.

Ellipsometry is made particularly attractive because of two factors: 1) it is not sensitive to variations in the absolute intensity of the light source, hence its non-perturbing character suitable for in-situ measurements, and 2) its remarkable sensitivity to surface,[2,3] such as the formation of a sparsely distributed sub-monolayer of atoms or molecules. As an example, the calculated results show that on a Si surface under the conditions of the calculation in Table 1.1, Δ changes by 0.3° per 0.1 nm of overlayer film.[5] Considering that a well aligned ellipsometer with high quality optics is capable of yielding Δ and Ψ values with a precision of about 0.01 - 0.02°,[4] submonolayer sensitivity is achievable. Another point to note is that, ellipsometric measurement requires only weak light sources, hence the incident light usually does not alter the surface. Ellipsometry has been shown to operate in air, vacuum and liquids, and the optical system can be positioned outside a processing environment. Thus, it can be used to monitor actual processes, hence it is non-invasive.

Table 1.1: Sensitivity of ellipsometry (conditions: film with index=1.5 on Si, λ=632.8 nm, ϕ=70°; sensitivity≈0.3° Δ per 0.1 nm film thickness)

Δ	Ψ	Thickness (nm)
179.257	0.448	0.0
178.957	0.448	0.1
178.657	0.449	0.2
178.357	0.450	0.3
178.056	0.451	0.4
177.756	0.453	0.5
176.257	0.462	0.6

The single wavelength ellipsometry (SWE) impacted semiconductors arena from the beginning of 1960s as a film thickness measurement technique applied to dielectric films on Si, and mostly for SiO_2 on Si.[6] In principle, the two measurable parameters, Δ and Ψ, at one wavelength λ and at an angle of incidence ϕ are sufficient to determine uniquely the film thickness L and refractive index n (when the assumption k=0 is made in the visible light range). The rapidly advancing technology requiring thinner films, multiple film stacks, films with complex and variable stoichiometries, and better precision of L and n, led most of us to the conclusion that SWE alone is inadequate for many important applications. Furthermore, questions arose about the use of a discreet single film model to analyze the measurable;[7] there are physical issues such as interface between film and substrate that is not as sharp and flat as one might think, and questions of stresses and stress gradients; there are chemical issues of stoichiometry and chemical gradients.[8] Each of these considerations added complexity to the ellipsometry measurement, requiring more measurable than afforded by SWE. The solution to this dilemma in terms of ellipsometry is straightforward: use of multiple λ and ϕ, i.e., all the accessible variables in order to specify a system-hence spectroscopic is required.

Except for the above case of dielectric film on Si or other materials of known optical constants, the only case for which the solution can be directly obtained from the two ellipsometric measurable, Δ and Ψ, at a special wavelength and an angle of incidence ϕ,

is a two-phase system where the material does not contain any overlayer. In this case, the dielectric function have a form[9)]

$$\langle\varepsilon\rangle = \sin^2\phi_0\left\{1+\tan^2\phi_0\left(\frac{1-\rho}{1+\rho}\right)^2\right\} \tag{1.1}$$

where ϕ_0 is the angle of incidence and ρ=tanΨexpΔ. The cleaved surface maintained in a N_2 atmosphere, in general, is thought to be closest to this realistic surface. However, it is difficult to produce the cleaved surface in a large size and ellipsometry is extremely sensitive to overlayer on the surface of a material, such as natural oxide layer and rough layer, hence the surface chemical treatment and clearing procedures become extremely important. The chemomechanical polishing adding the chemical etching is the most effective technology for the Si, Ge, and III-V semiconductors, which can produce the sharpest substrate-ambient discontinuities, that is, the minimum amount of interface material will be left at their surface.[10,11)] The spectroscopic ellipsometric measurements of the pseudo (apparent) dielectric function $\langle\varepsilon\rangle = \langle\varepsilon_1\rangle + i\langle\varepsilon_2\rangle$ of semiconductors at the wavelength of the E_2 peak of $\langle\varepsilon_2\rangle$ provide direct information about the state of the surface. But, in order to prevent from re-oxidization and surface contamination effects, it is necessary to maintain sample in a N_2 flow during the measurements.[12,13)] Other method, which is simple in technique and is widely used, is the mathematics stripping procedures, i.e. the overlayer is removed according to the mathematics management. In this procedure, the precise optical constants of the oxide must be known beforehand.[14)]

In many cases, the solution of parameters for the samples, such as dielectric function and thickness of film can not be directly calculated from the ellipsometric measurements. Therefore, many efforts in spectroscopic ellipsometry are focused on analyzing the data using the Fresnel equations, that is, the unknown parameters of samples are determined by least squares minimization of the difference between the calculated and experimental values of Δ and Ψ using a suitable model. As a figure of merit for comparison, an unbiased estimator δ is calculated from the relationship:[15)]

$$\delta^2 = \frac{1}{N-P-1}\sum_{i=1}^{N}\left|\rho_i^{\exp}-\rho_i^{cal}\right|^2, \tag{1.2}$$

where N is the number of wavelengths sampled and P is the number of unknown parameters. The unknown optical constants of materials is often described as a simple dispersion, such as Cauchy formulae[16)]

$$n(\lambda) = n_0 + n_2/\lambda^2 + n_4/\lambda^4 \tag{1.3}$$
$$k(\lambda) = k_0 + k_1/\lambda + k_3/\lambda^3,$$

where n_0, n_2, n_4, k_0, k_1 and k_3 are fitting parameters and λ is wavelength, and a single oscillator model is used as follows;[17)]

$$\varepsilon = \varepsilon'_\infty + \frac{(\varepsilon_s - \varepsilon'_\infty)\,\omega_t^2}{\omega_t^2 - \omega^2 + i\Gamma_0\omega}, \tag{1.4}$$

where ε'_∞ represents the high-frequency dielectric constant, ε_s the oscillator strength, ω_t the frequency and Γ_0 the damping factor of the oscillator. The Bruggeman effective medium approximation (BEMA) has been shown to be quite useful for calculating the dielectric response of mixed composition inhomogeneous films. BEMA assumes mixtures on a scale smaller than the wavelength of light, but that each constituent retains its original dielectric response. One can imagine that this model may be appropriate for mixed phase films and for substrate with large amounts of impurities and damage. The generalized form for the BEMA is[18)]

$$\sum_i f_i \frac{\varepsilon_i - \varepsilon}{\varepsilon_i + 2\varepsilon} = 0, \tag{1.5}$$

where ε is the composite dielectric function and ε_i and f_i are the dielectric function and volume fraction respectively of the ith constituent.

Spectroscopic ellipsometry is also a powerful tool to characterize the electronic structure and its temperature dependence of semiconductors. Many analytical model have been developed for this purpose, such as the harmonic oscillator model of Erman et. al., the dielectric function $\varepsilon(\omega)$ is given by[19)]

$$\varepsilon(\omega) = 1 - \sum_{k=1}^{n} A_k \left(\frac{1}{\hbar\omega - E_k + i\Gamma_k} - \frac{1}{\hbar\omega + E_k + i\Gamma_k} \right). \tag{1.6}$$

where E_k is the energy of a harmonic oscillator and Γ_k is its linewidth. And the standard

analytic line shapes:[20]

$$\varepsilon(\omega) = 1 - \sum_{k=1}^{n} A_k e^{i\phi_k} (\hbar\omega - E_k + i\Gamma_k)^n, \tag{1.7}$$

where the critical points (CP's) are described by the amplitude A_k, threshold energy E_k, broadening Γ_k, and the excitonic phase angle ϕ_k. The exponent n has the value -1/2 for one-dimensional (1D), 0 [logarithmic, i.e., $ln(\omega - E + i\Gamma)$] for 2D, and 1/2 for 3D CP's. Discrete excitons are represented by n=-1. For the practical purpose, the standard analytic line shapes often use its second-derivative form to fit numerically the second derivative of the dielectric function with respect to photon energy $d_2\varepsilon/d\omega_2$.

In summary, spectroscopic ellipsometry is at once a nondestructive, non-contact and powerful optical technique to investigate surface and physical characteristics of materials and is an indirect measuring tool. The data analysis is a hard task and requires powerful mathematical tool.

1.2 Organization of dissertation

The dissertation is composed of seven chapters, and each of them is summarized as follows.

Chapter 1, which is an introduction of this dissertation, reviews the historical development and describes the characteristic and main research areas of spectroscopic ellipsometry. The models, which are widely used in data analysis of SE, are also summarized.

In chapter 2, the measurement principles of rotating-analyzer system are described in detail. The general mathematical representation of ellipsometry for the multilayer structure that includes Fresnel equations are also given. Levenberg-Marquardt algorithm, which is widely used in spectroscopic ellipsometry, is also described in detail. Our proposed model "Modified Harmonic Oscillator Approximation Scheme" as well as several other theoretical models to describe optical respond of semiconductor are introduced.

In chapter 3, the characterization of III-V semiconductors, such as, GaP and GaAs, grown on Si substrate by metal-organic chemical-vapor deposition (MOCVD) are studied. The difference between the band E_1 energy of the epitaxial GaP on Si substrate and bulk

GaP decreases with increasing thickness of epitaxial GaP resulting from the stress varying with the thickness. For the thick GaAs film on Si, the stress in GaAs film and the rough layer on surface have been investigated according to the direct analysis for the SE data and surface mechanochemical polishing of GaAs layers. The results of surface roughness are compared between SE and that obtained by AFM.

In chapter 4, characterization results of excimer laser annealed polycrystalline Si and $Si_{1-x}Ge_x$ alloy thin films are described. Two kind of samples have been used in the experiment. One, a structure of α-Si/SiO_2/Si-substrate deposited by LPCVD, and the other is α-$Si_{1-x}Ge_x$ on Si and glass substrate deposited by ion-beam sputtering. The threshold energy for the crystallization to occur, the volume fraction of crystalline and density varying with increasing the laser irradiation energy are discussed. A method to estimate the compositions of $Si_{1-x}Ge_x$ alloy films is also proposed. The results of the compositions and grain size of poly-$Si_{1-x}Ge_x$, which are determined by SE as well as X-ray, have been compared.

In chapter 5, the optical and mechanical properties of GaN grown on sapphire substrate are investigated by spectroscopic ellipsometry, transmission method and depth-sensing indentation experiments. The optical constants and "true hardness" of GaN film are first accurately determined. The optical properties of $Al_xGa_{1-x}N$ embedded in the structure, $Al_xGa_{1-x}N$/GaN/Sapphire, is then determined by simultaneous fitting of SE data at three angles of incidence, 40°, 50° and 60°.

In chapter 6, the evaluation method of SE together with transmission method is successfully applied to inhomogeneous films such as sol-gel derived TiO_2 films on quartz and silicon substrates. Unlike the usual practice data analysis where the refractive index is assumed to vary, it assumed for the first time that the volume fraction of void linearly varies from the outer surface to inner surface of the inhomogeneous film. The accurate refractive index and absorbent coefficient over the wavelength range of 300 - 1600 nm have been obtained by using both SE and transmission method.

Chapter 7 is the summary of this dissertation where a scope for future work is also given.

References

[1] J. Jamin, Ann: chim. phys., **29**, 263 (1850).

[2] P. Drude, Ann. Phys. Chem., **36**, 532, 865 (1889).

[3] D. E. Aspnes and A. A. Studna, Appl. Phys. Lett., **39**, 316 (1981).

[4] D. E. Aspnes and A. A. Studna, Appl. Opt., **14**, 220 (1975).

[5] J. De Laet, J. Vanhellemont, H. Terryn and J. Vereecken, Thin Solid Films, **233**, 58 (1993).

[6] R. J. Archer, J. Opt. Soc. Am., **52**, 970 (1962).

[7] J. B. Theeten and D. E. Aspnes, Thin Solid Films, **60**, 193 (1979).

[8] E. A. Irene, in J. E. Greene (ed.), CRC Critical Reviews in Solid State and Materials Science, Vol 14 (2), 175-223 (1988).

[9] R. M. A. Azzam and N. M. Bashara, Ellipsometry and Polarized Light (North-Holland, Amsterdam, 1977).

[10] D. E. Aspnes and A. A. Studna, Appl. Phys. Lett., **39**, 316 (1981).

[11] D. E. Aspnes and A. A. Studna, Phys. Rev. B **27**, 985 (1983).

[12] K. Utani and S. Adachi, Jpn. J. Appl. Phys., **32** 3572 (1993).

[13] G. Yu, T. Soga, J. Watanabe, T. Jimbo and M. Umeno, Jpn. J. Appl. Phys. **36**, 2829 (1997).

[14] P. Lautenschlager, M. Garriga, S. Logothetidis and M. Cardona, Phys. Rev. B **35** 9174 (1987).

[15] D. E. Aspnes, J. B. Theeten and F. Hottier, Phys. Rev. B, **20**, 3992 (1979).

[16] F. Ferrieu and J. H. Lecat, J. Electrochem. Soc., **137**, 2203 (1990).

[17] T. Gerfin and Michael Grätzel, J. Appl. Phys., **79** 1722 (1996).

[18] D. A. G. Bruggemann, Ann. Phys. (Leipzig), **24** (1935).

[19] M. Erman, J. B. Theeten, N. Vodjdani and Y. Demay, J. Vac. Sci. Technol., B, **1**, 328 (1983).

[20] M. Cardona, Modulation Spectroscopy, Suppl. 11 of Solid State Physics, edited by F. Seitz, D. Turnbull and H. Ehrenreich (Academic, New York, 1969).

Chapter 2

Theory and Experiment

2.1 Introduction

Given a set of measured data of SE, which are often reduced to the complex Fresnel reflection coefficient ratio (Eq. 2.1), one often want to condense and summarize the data by fitting it to a "model" that depends on adjustable parameters. Sometime, the parameters are simply a set of films thicknesses. Other times, the parameters include not only the film thickness, but also some underlying theory as described in next section.

$$\rho(\lambda, \phi) = r_p/r_s = \tan \Psi(\lambda, \phi) \exp i\Delta(\lambda, \phi) \tag{2.1}$$

where $r_p(r_s)$ represents the complex Fresnel reflection ratio for light polarized parallel (perpendicular) to the plane of incidence. The angle Ψ and Δ are the conventional ellispometry parameters normally associated with nulling ellipsometry techniques.[10] The ratio ρ, as well as Ψ and Δ, depends explicitly on the wavelenth λ and angle of incidence ϕ.

The data in the form of Eq. 2.1 (or possibly some other, equivalent form) are then compared with a calculated spectrum, where the figure of merit is generally chosen to be the unbiased estimator,[11] given by

$$\begin{aligned} \chi_u^2 &= \frac{1}{n-p-1} \sum_{i=1}^{n} \Big[(\tan \Psi_{\exp}(\lambda_i) - \tan \Psi_{calc}(\lambda_i, \mathbf{z}))^2 \\ &+ (\cos \Delta_{\exp}(\lambda_i) - \cos \Delta_{calc}(\lambda_i, \mathbf{z}))^2 \Big] \end{aligned} \tag{2.2}$$

The vector $\mathbf{z}$ (with m components) represents the parameters in the calculation model. The fitting procedure usually used to minimize χ_u^2 with a numerical analysis method is

Levenberg-Marquardt Method.[12] In Eq. 2.2 there is no attempt to weight the data spectrally in determined the figure of merit of the fit by using the error in the experiment quantity ρ.

Spectroscopic ellipsometry (SE) has been used for nondestructive determination of thicknesses and alloy compositions,[13] and evaluation of strained epilayers of semiconductor.[14,15] However, in order to determine the parameters of the electronic band structure of a material in a given structure, the complex dielectric function of that material must be known as a function of the parameters of the electronic band structure.[15] The standard critical-point model has been widely used to fit second numerical the derivatives of the dielectric function with respect to photon energy for indirect transition semiconductor, such as Si[15,16] and GaP[15,17] and to determine electronic critical-point energies E_j and line shapes of Si and GaP. However, it is not valid for the dielectric function. The harmonic oscillator approximation (HOA) can approximate the dielectric response of single-crystal $Al_xGa_{1-x}As$ using the minimum number of parameters for photon energies above the fundamental band edge. It has been used to study GaAs/GaAlAs quantum well structure[18] and ion-damaged GaAs.[19] However, the HOA model is not related to band structure and fails to fit the number derivatives of the dielectric function with respect to photon energy. Recently, Terry has substantially improved the HOA model by allowing the contribution of each oscillator to have an arbitrary phase angle.[20] However, even this improved version of the HOA model still suffers from the weaknesses stated above. Recently, Kim et al. developed a new model for the dielectric function of zincblende semiconductors in which the joint density of states between a pair of bands ($J_{cv}(E)$) is written as the the product of a function of E which gives the correct critical-point (CP) analytic properties and a low -order polynomial in E. Kim et al. have obtained excellent simultaneous fits to $\varepsilon(\omega)$ of GaAs and its first three numerical derivatives with respect to energy, and accurate values of the critical-point energies and line widths.[21] However, this model involves complicated mathematical formula and requires much computational effort.

In this chapter, the complex Fresnel reflection coefficient ratio dependence on the structure parameters of samples, such as complex refractive index and thickness, are given,

and Levenberg-Marquardt Method using the SE data analysis and error estimates on the parameters are described. Our modified HOA model have been particularly mentioned, which give the excellent simultaneous fits to $\varepsilon(\omega)$ of GaAs, InP and GaP and their first three numerical derivatives with respect to energy without much computational effort. The other important analytic model have also been described.

2.2 The concept and measurement of elliptical polarization

2.2.1 The concept of elliptical polarization

For a uniform monochromatic TE (transverse-electric) plane wave along the direction z, at a fixed point in space the vibration of the electric vector E can be resolved into two independent, linear, simply-harmonic vibrations, E_x and E_y, along two mutually orthogonal directions, x and y, respectively.

$$E = E_x\hat{\mathbf{x}} + E_y\hat{\mathbf{y}} \tag{2.3}$$

$$E_i = A_i \cos(\omega t + \delta_i), \qquad i = x, y \tag{2.4}$$

$\hat{\mathbf{x}}$, $\hat{\mathbf{y}}$ are unit vectors along the coordinate axes; A_i and δ_i represent the amplitude and phase, respectively, of the linear vibration along the ith coordinate axis and ω represents the angular frequency.

The special case of $\delta_x = \delta$ and $\delta_y = 0$ is first discussed and it is proved that if $\delta \neq 0$, the end-point of the electric vector will trace an ellipse in xy plane.[1)] Such an ellipse is periodically described at a repetition rate equal to the optical frequency $f = \omega/2\pi$. Further, it will be proved that the general form as eq. 2.4 can be changed into special form by a coordinate rotation.

In the case of $\delta_x = \delta$ and $\delta_y = 0$, eq. 2.4 takes the form

$$\begin{aligned} E_x &= A_x \cos\delta \cos\omega t + A_y \sin\delta \sin\omega t, \\ E_y &= A_y \cos\omega t. \end{aligned} \tag{2.5}$$

By elimination of t from eq. 2.5, it is found that the coordination (E_x and E_y) of the end-point of electric vector satisfy the following equation

$$\frac{E_x^2}{A_x^2 \sin^2 \delta} + \frac{E_y^2}{A_y^2} - \frac{2\cos\delta}{A_x A_y \sin^2 \delta} E_x E_y = 1 \tag{2.6}$$

which is the equation of an ellipse in the xy plane. By a coordinate rotation, the azimuth (orientation) of the major axis of the ellipse and the lengths of the semi-major and the semi-minor axes can all be determined in terms of A_x, A_y and δ.[2)]

In the general case, that is $\delta_x \neq \delta_y \neq 0$ in eq. 2.4, we resolve that each of the two linear vibrations in eq. 2.4 into two colinear vibrations, in time-quadrature with one another, along the same axis

$$E_i = (A_i \cos\delta_i)\cos\omega t - (A_i \sin\delta_i)\sin\omega t, \qquad i = x, y. \tag{2.7}$$

The electric vector E in eq. 2.3 can be written as

$$\begin{aligned} E &= (A_x \cos\delta_x \hat{\mathbf{x}} + A_y \cos\delta_y \hat{\mathbf{y}})\cos\omega t - (A_x \sin\delta_x \hat{\mathbf{x}} + A_y \sin\delta_y \hat{\mathbf{y}})\sin\omega t \\ &= (a_1 \cos\omega t)\,\hat{\mathbf{u}}_1 - (a_2 \sin\omega t)\,\hat{\mathbf{u}}_2 \end{aligned} \tag{2.8}$$

In this equation $\hat{\mathbf{u}}_1$ and $\hat{\mathbf{u}}_2$ represent unit vectors along the directions of $\cos\omega t$ and $\sin\omega t$ vibration and a_1 and a_2 represent their respective amplitudes. a_1, a_2, $\hat{\mathbf{u}}_1$ and $\hat{\mathbf{u}}_2$ are given by

$$\begin{aligned} a_1 &= \sqrt{A_x^2 \cos^2\delta_x + A_y^2 \cos^2\delta_y} \\ a_2 &= \sqrt{A_x^2 \sin^2\delta_x + A_y^2 \sin^2\delta_y} \\ \hat{\mathbf{u}}_1 &= a_1 \left(\frac{A_x \cos\delta_x}{a_1}\hat{\mathbf{x}} + \frac{A_y \cos\delta_y}{a_1}\hat{\mathbf{y}} \right) \\ &= a_1 (\cos\theta_1 \hat{\mathbf{x}} + \sin\theta_1 \hat{\mathbf{y}}) \end{aligned}$$

and

$$\begin{aligned} \hat{\mathbf{u}}_2 &= a_2 \left(\frac{A_x \sin\delta_x}{a_2}\hat{\mathbf{x}} + \frac{A_y \sin\delta_y}{a_2}\hat{\mathbf{y}} \right) \\ &= a_2 (\cos\theta_2 \hat{\mathbf{x}} + \sin\theta_2 \hat{\mathbf{y}}) \end{aligned} \tag{2.9}$$

Taking a coordinate rotation with an angle of rotation θ_2 with the help of Fig. 2.1, and

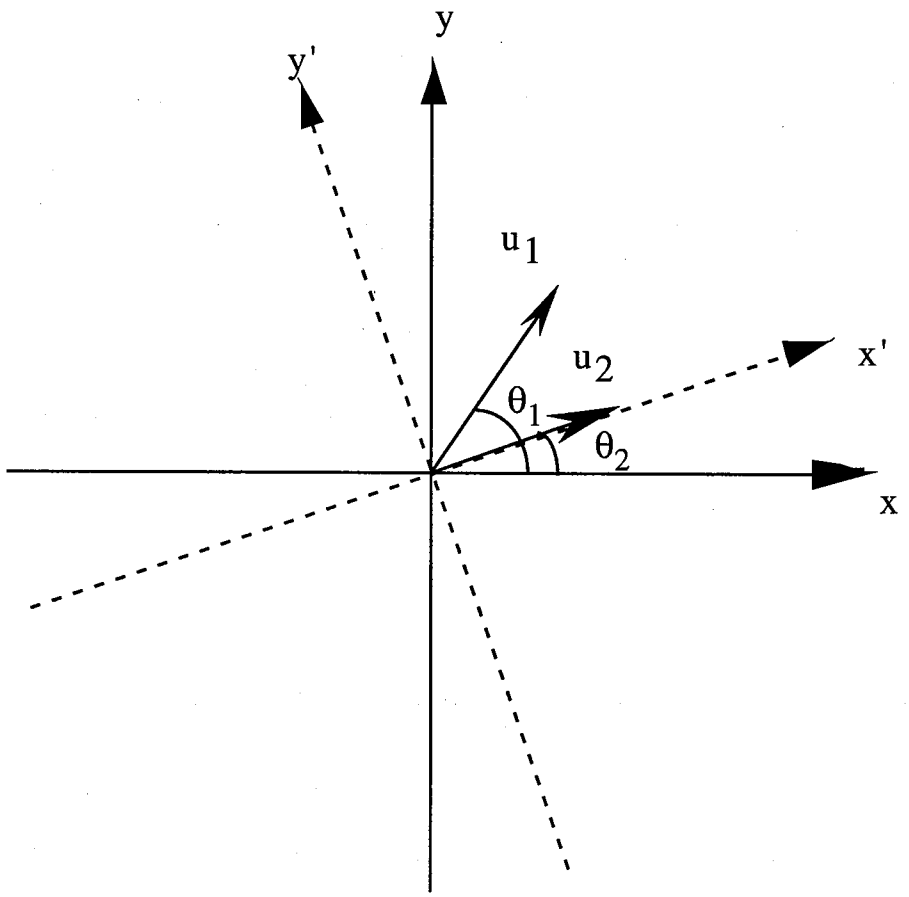

Figure 2.1: The coordinate rotation transform with the angle of rotation θ_1

the projections of electric vector E parallel ($||$) and perpendicular ($\perp$) to $\hat{u}_2$ we get

$$\begin{aligned} E_{||} &= (a_1 \cos(\theta_1 - \theta_2)) \cos\omega t - a_2 \sin\omega t = \sqrt{a_1^2 \cos^2(\theta_1 - \theta_2) + a_2^2} cos(\omega t + \delta') \\ E_{\perp} &= (a_1 \sin(\theta_1 - \theta_2)) \cos\omega t. \end{aligned} \tag{2.10}$$

In this equation δ' is given by

$$\cos\delta' = \frac{a_1 \cos(\theta_1 - \theta_2)}{\sqrt{a_1^2 \cos^2(\theta_1 - \theta_2) + a_2^2}}. \tag{2.11}$$

The eq. 2.10 have the same form as the eq. 2.5. So far we have proved that the elliptical (or elliptic) polarization is the most general state of polarization of any optical filed that is strictly monochromatic. For complete specification of the elliptical state we need to know

(1) The amplitude (size) of the ellipse;

(2) The absolute temporal phase.

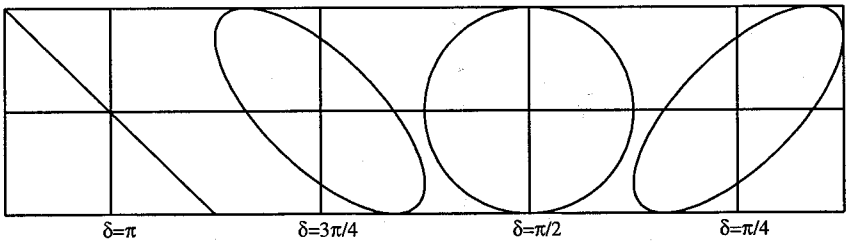

Figure 2.2: The ellipses of polarization with some especially difference of phase

In Fig. 2.2 we plot the end-point trace of the electric vector for the case of $\delta_x = \delta_y$ and for some other differences of phase. It is obvious that the states of linear ($\delta = k\pi$) and circular polarization ($\delta = (2k+1)\pi/2$) are only limiting cases of the more general state of elliptical polarization.

2.2.2 The measurement of elliptical polarization

Ellipsometers differ in the way in which the polarization of reflected light is measured. Most instruments now use photometric SE, where the intensity of the reflected light is measured while modulating the polarization of the incident or reflected light. Photometric ellipsometer system possess a number of advantages over those of classical null design.[3-5] The high optical efficiency of photometric systems allows operation with much weaker (e.g., continuum) light sources without sacrificing shot noise or source instability detection capability which in turn permits wavelength scanning to high precision. Furthermore, operation can be made automatic in the sense usually applied to ellipsometer system: complex reflectance data can be obtained by direct analog or digital analysis of the time dependence of the transmitted flux, and the operator is thereby removed as an essential feedback element in the measurement process.

Figure 2.3 shows the main components of an ellipsometer. A monochromator is inserted in the input or output line for SE. The compensator is a phase-shifting element which is essential for null-ellipsometers. Two types of modulation are used: the polarizer, analyzer or compensator can be rotated, or the phase shift of the compensator can be varied with a photoelastic modulator (PEM), where a strain-induced birefringence in quartz glass is used to modulate the polarization. Both types of systems are capable of substantially

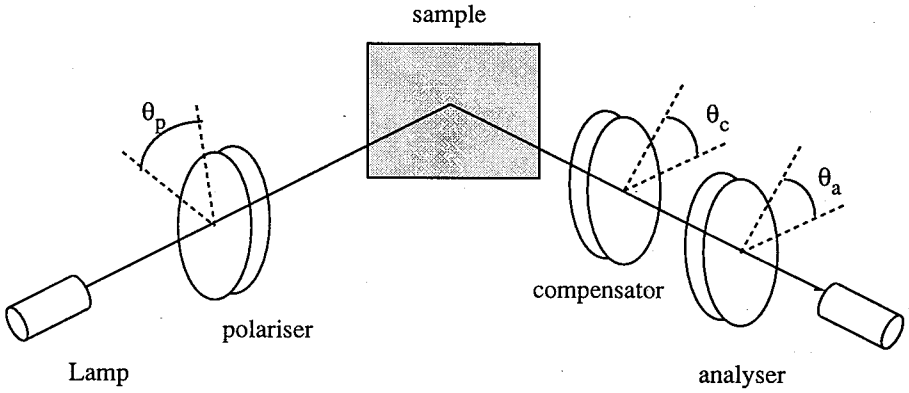

Figure 2.3: Schematic of the main components of an ellipsometer

greater precision than null systems, partly because shot-noise detection conditions are much easier to achieve with currently available source, but primarily because no precision-limiting quantized mechanical motions are involved in the measurement process. Rotating-analyzer systems have the advantages of simplicity and relative insensitivity to wavelength in scanning applications, while piezobirefringent element system have the advantage of high speed.[5-7)]

The spectra studied here were taken with rotating-analyzer system. The light sources used are 75 W Xe high pressure arc-lamps, which has a continuous spectrum between 1.5 eV (830 nm) and 6.2 eV (200 nm). An angle of incidence, ϕ_0, between 40° and 90° provides highest sensitivity to film properties for semiconductor substrates. Photomultiplier detectors are used, with their advantages of high quantum efficiency in the visible and near UV spectral region, high gain, and an extremely linear relationship between light intensity and signal.

The analyzer rotates at a constant frequency to limit mechanical vibration. The angle of the transmission axis of the analyzer is measured by an angle encoder or resolver mounted on the holder of the analyzer. For absorbing materials, the reflected light is elliptically polarized, which produces a sinusoidal varying intensity when the analyzer is rotated.[6)]

As above-mentioned the general elliptical polarization can be described as:

$$\begin{aligned} E_x &= A_x \sin(\omega t + \delta_x) \\ E_y &= A_y \sin(\omega t + \delta_y). \end{aligned} \tag{2.12}$$

The intensity I(A) at the detector is

$$\begin{aligned} I(A) &= \frac{1}{T}\int_0^T E^2 dt \\ &= \frac{1}{T}\int_0^T \left(A_x \sin(\omega t + \delta_x)\cos\theta_A + A_y \sin(\omega t + \delta_y)\sin\theta_A\right)^2 dt \\ &= \frac{A_x^2}{2}\cos^2\theta_A + \frac{A_y^2}{2}\sin^2\theta_A + A_x A_y \cos(\delta_x - \delta_y)\sin\theta_A\cos\theta_A \\ &= \frac{A_x^2}{4}(\cos 2\theta_A + 1) + \frac{A_y^2}{4}(1 - \cos 2\theta_A) + \frac{A_x A_y}{2}\cos(\delta_x - \delta_y)\sin 2\theta_A \\ &= \frac{A_x^2 + A_y^2}{4} + \frac{A_x^2 - A_y^2}{4}\cos 2\theta_A + \frac{A_x A_y}{2}\cos(\delta_x - \delta_y)\sin 2\theta_A \\ &= I_0\left(1 + a_2 \cos 2\theta_A + b_2 \sin 2\theta_A\right). \end{aligned} \tag{2.13}$$

This is a function of the time-varying angular position of the transmission axis of the analyzer, θ_A (Fig. 2.3). The coefficients a_2 and b_2 are obtained by a Fourier transform of the intensity and in the case of Figure 2.3 without the compensator, are calculated according to the expression

$$\begin{aligned} a_2 &= \frac{A_x^2 - A_y^2}{A_x^2 + A_y^2} = \frac{\tan^2\Psi\cos^2\theta_P - \sin^2\theta_P}{\tan^2\Psi\cos^2\theta_P + \sin^2\theta_P} \\ b_2 &= \frac{\cos\Delta\tan\Psi\sin 2\theta_P}{\tan^2\Psi\cos^2\theta_P + \sin^2\theta_P}. \end{aligned} \tag{2.14}$$

The relation of $A_x/A_y = \tan\Psi\cos\theta_P/\sin\theta_P$ and $\delta_x - \delta_y = \Delta$ has been used in the calculation. An important advantage of photometric SE is that it is not sensitive to variations in the absolute intensity of the light source because the Fourier coefficients are calculated from relative intensities. A second point to note is that, because maxima occur twice per revolution, the first and third harmonics of the Fourier expansion should be zero, and this can be used as a check on alignment. These components can be reduced to less than 0.002.[8)]

The measurement processing step involves the calculation of the normalized Fourier transform coefficients (a_2, b_2) of the signal voltage from the accumulated data that have been stored as N data words. These normalized Fourier coefficients are calculated according to the expression[7)]

$$a_2 + ib_2 = 2\left[\sum_{i=1}^{N} D_i \exp(2iA_i)\right] \Big/ \left(\sum_{i=1}^{N} D_i\right) \tag{2.15}$$

where D_i, i=1,2, ... , N are the data words representing the sum over the total number of cycles of the signal values measured at the N reading points of a single cycle, and

$$A_i = \pi\,(i-1)\,/36$$

2.3 The general formula for ellipsometry

2.3.1 The polarized state of reflection at an interface between medium 1 and medium 2

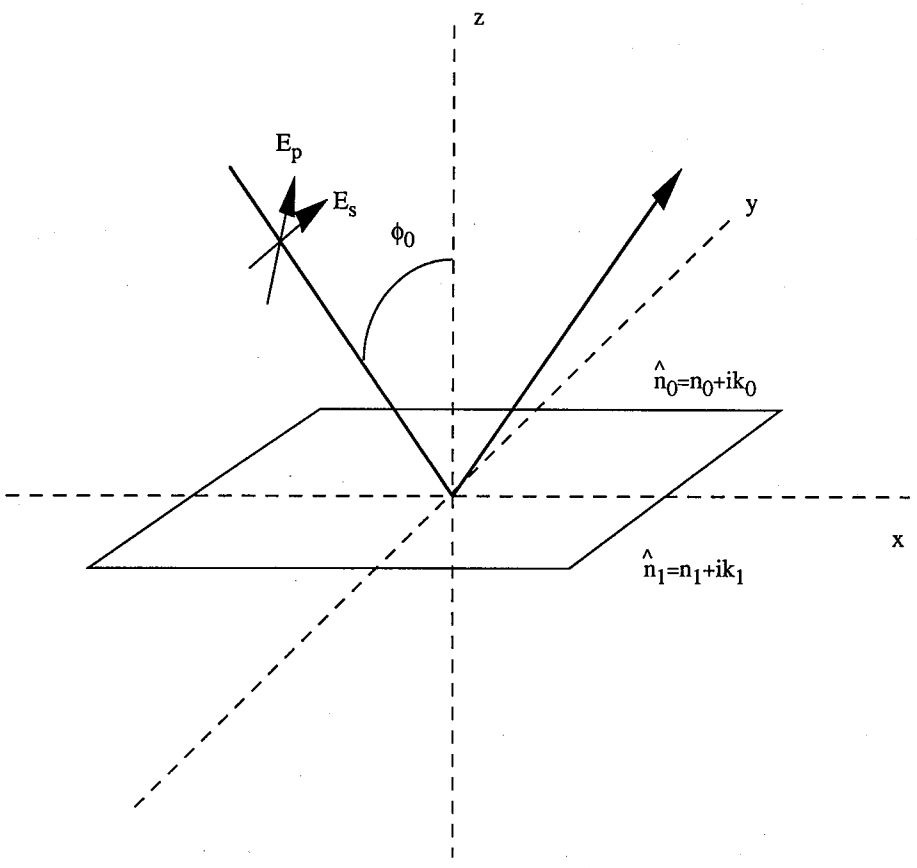

Figure 2.4: Interface geometry

The geometry of interface is shown in Fig. 2.4, where both the mediums have complex index ($\hat{n} = n+ik$). The p-polarization describes an electric vector in the plane of incidence

(the xy-plane), and a s-polarization describes an electric vector in the y-direction. The angle of incidence is ϕ_0.

Applying the boundary conditions at the interface yields the well-known Fresnel equation for the (complex) amplitude of the reflected wave as follow,

$$\begin{aligned} \hat{r}_p &= \frac{\hat{n}_1 \cos\phi_0 - \hat{n}_0 \cos\hat{\phi}_1}{\hat{n}_1 \cos\phi_0 + \hat{n}_0 \cos\hat{\phi}_1} = |\hat{r}_p|\, e^{i\delta_p}, \\ \hat{r}_s &= \frac{\hat{n}_0 \cos\phi_0 - \hat{n}_1 \cos\hat{\phi}_1}{\hat{n}_0 \cos\phi_0 + \hat{n}_1 \cos\hat{\phi}_1} = |\hat{r}_s|\, e^{i\delta_s}, \\ \cos\hat{\phi}_1 &= \frac{1}{\hat{n}_1}\sqrt{\hat{n}_1^2 - \hat{n}_0^2 \sin^2\phi_0}. \end{aligned} \tag{2.16}$$

As it has been discussed in the section 2.2, the light of reflection has an elliptically polarized state. The general ellipsometric parameters are represented by the ratio of amplitudes ($\tan\Psi$) and difference of phase (Δ) between the p-polarization and s-polarization. Its mathematical form is represented as:

$$\hat{\rho} = \frac{\hat{r}_p}{\hat{r}_s} = \frac{|r_p|}{|r_s|} e^{i(\delta_p - \delta_s)} = \tan\Psi e^{i\Delta} \tag{2.17}$$

An important, special case is that of a light reflection between the vacuum and the surface of a medium. In this case the index of vacuum is one and the dielectric function of medium is $\varepsilon = (n + ik)^2$, and eq. 2.16 become:

$$\begin{aligned} \hat{r}_p &= \frac{\sqrt{\varepsilon}\cos\phi_0 - \cos\hat{\phi}}{\sqrt{\varepsilon}\cos\phi_0 + \cos\hat{\phi}}, \\ \hat{r}_s &= \frac{\cos\phi_0 - \sqrt{\varepsilon}\cos\hat{\phi}}{\cos\phi_0 + \sqrt{\varepsilon}\cos\hat{\phi}}, \\ \cos\hat{\phi} &= \frac{1}{\sqrt{\varepsilon}}\sqrt{\varepsilon - \sin^2\phi_0}. \end{aligned} \tag{2.18}$$

The ellipsometric parameters Ψ and Δ are given by

$$\rho = \tan\Psi e^{i\Delta} = \frac{\sqrt{\varepsilon}\cos\phi_0 - \cos\hat{\phi}}{\sqrt{\varepsilon}\cos\phi_0 + \cos\hat{\phi}} \Big/ \frac{\cos\phi_0 - \sqrt{\varepsilon}\cos\hat{\phi}}{\cos\phi_0 + \sqrt{\varepsilon}\cos\hat{\phi}}. \tag{2.19}$$

From the eq. 2.19 the dielectric function of medium ε can be represented as the function of ellipsometric parameters Ψ and Δ.

$$\varepsilon = \sin^2\phi_0 \left(1 + \tan^2\phi_0 \frac{(\rho - 1)^2}{(\rho + 1)^2}\right) \tag{2.20}$$

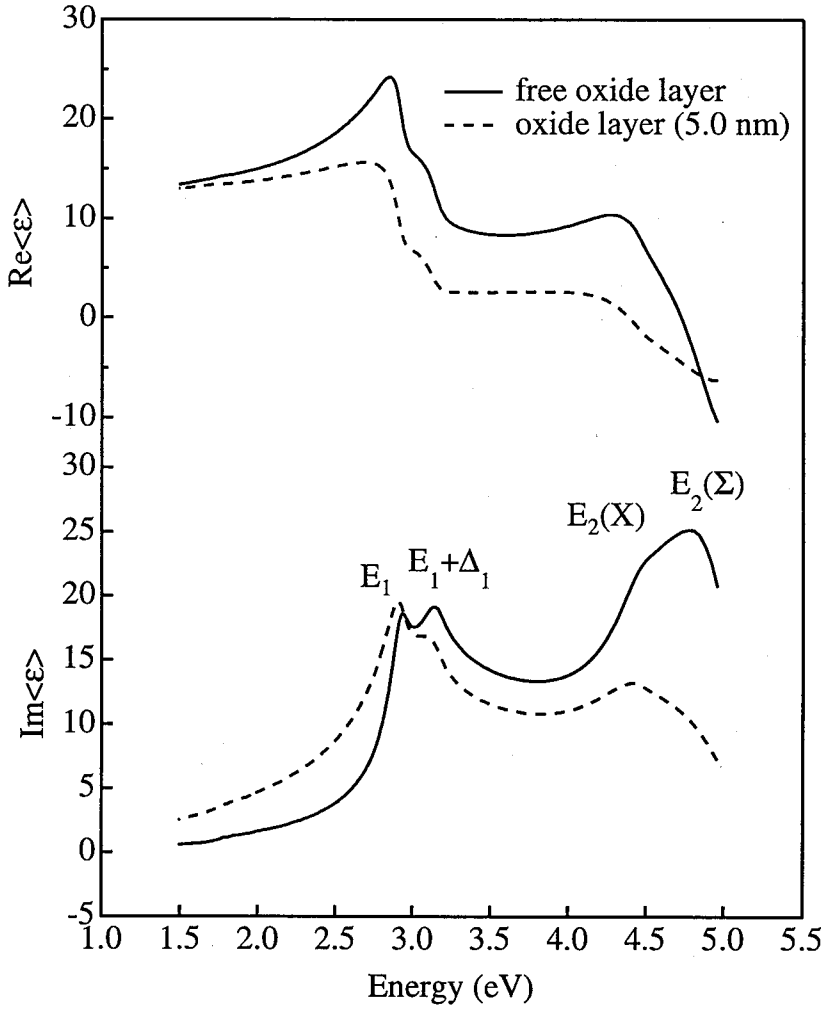

Figure 2.5: The relation between the oxide layer on surface and pseudo-dielectric function. The solid lines are the pseudo-dielectric function of the free oxide surface of GaAs, and the dashed line are that for 5.0 nm oxide layer covering on the surface of GaAs.

Thus, if Ψ and Δ are known by measurement, the dielectric function ε of a medium can be only determined by using eq. 2.20. This dielectric function is the (complex) bulk dielectric function of a homogeneous material without the surface overlayer (two-phase model). Such an ideal condition is not usually satisfied in real environment but, even for the isotropic materials, surface reconstruction, roughness and contamination may render the two-phase model invalid. The dielectric function determined by eq. 2.20 is then an average over the region penetrated by the incident light and, in equation 2.20, ε becomes $\langle\varepsilon\rangle$, the pseudo-or effective dielectric function. This pseudo-dielectric function can be used to evaluate the quality of the surface of a material. In the Fig. 2.5 we show the oxide layer on surface

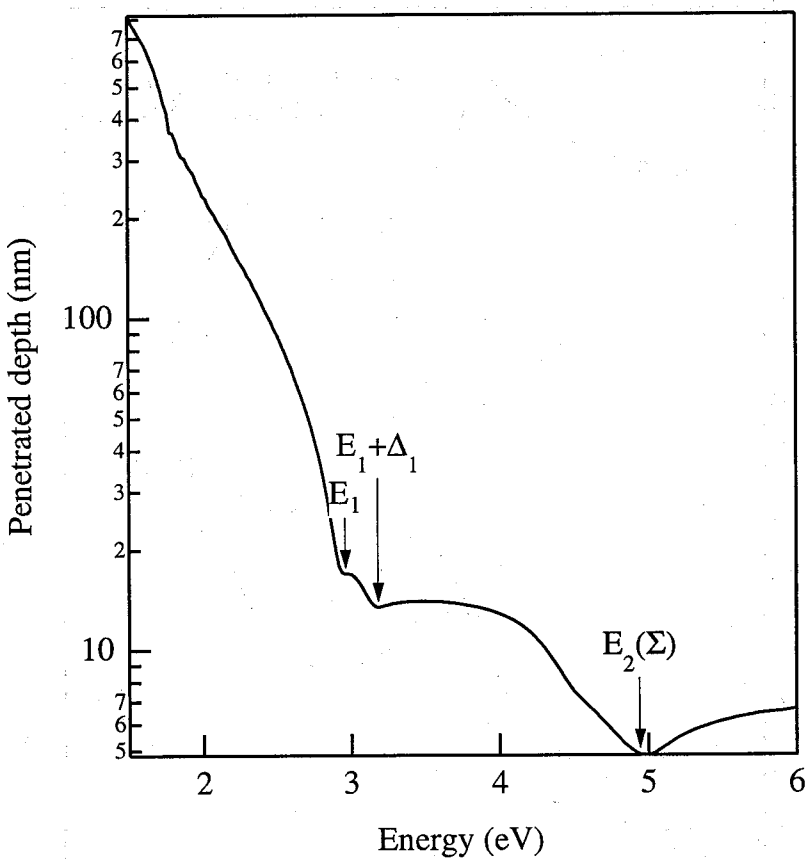

Figure 2.6: The penetrated depth of light from the GaAs surface

of GaAs effecting on the pseudo-dielectric function obtained by spectroscopic ellipsometry. In the figure four peaks are obviously observed in the spectra of imaginary part of the pseudo-dielectric function $\langle\varepsilon\rangle$, which are attributed to $E_1\,(L_3^v \rightarrow L_3^c)$ and $E_2\,(X_4^v \rightarrow X_1^c)$ interband transitions (mentioned in the following chapter).

Fig. 2.6 shows that the depth penetrated by the incident light calculated using the absorption coefficient of GaAs over the photon energy range of 1.5 - 6 eV. In the figure the smallest penetrated depth is about 5.0 nm, which occur near the E_2 energy (4.8 eV). Hence, it is concluded that the peak value of imaginary part ε_2 of pseudo dielectric function at the energy of the E_2 band provide a sensitive and unambiguous indication of the sharpness of the dielectric discontinuity between the substrate and ambient, responding not only to residual oxides and other overlayers but also to the selvedge region, bulk degradation, and microstructural effects as well. D. E. Aspnes et. al. proposed a method to produce

Table 2.1: Chemical treatments yielding the sharpest dielectric discontinuity between bulk and ambient.

Material	Pretreatment	Etch/polish	Strip	ε_2 peak (Energy eV)
Si ⟨111⟩	Syton	BRM pad	BRM, HF5, AMH, HF5	48.05 (4.25)
⟨110⟩	Syton	BRM pad	BRM, BHF/MeOH	44.75 (4.25)
⟨100⟩	Syton	BRM pad	BRM, HF5	44.62 (4.25)
Ge ⟨111⟩	Syton	BRM pad	BRM, BHF	30.74 (4.25)
⟨110⟩	Syton	BRM pad	BRM, BHF	29.93 (4.25)
⟨100⟩	Syton	BRM pad	BRM, BHF	30.53 (4.25)
GaP ⟨110⟩	Br-meth	BRM pad	BRM, H_2O, AMH	27.09 (5.05)
GaAs⟨100⟩	Br-meth	BRM pad	AMH, BRM, H_2O	25.59 (4.78)
GaSb⟨111⟩	Br-meth	BRM pad	BRM, H_2O	25.28 (4.03)
InP ⟨100⟩	Br-meth	BRM pad	BRM, H_2O, AMH	23.00 (4.71)
InAs⟨110⟩	Tizox	BRM pad	AMH, BRM, H_2O, AMH	22.81 (4.44)
InSb⟨110⟩	Tizox	BRM pad	BRM	20.89 (3.85)
InSb⟨100⟩	Tizox	BRM pad	BRM	20.12 (3.85)

BRM pad: 0.05-vol % bromine in methanol; chemomechanical polish on lens paper for 20 s full strength followed by 10 s dilution to methanol.
BRM: 0.05-vol % bromine in methanol, followed by methanol rinse.
AMH: 1:1-vol NH_4OH in H_2O, followed by H_2O rinse.
BHF: buffered HF, followed by H_2O rinse (exception: final rinse, Si ⟨110⟩).
HF5: 5-vol % HF in methanol, followed by methanol rinse.
MeOH: methanol.

most abrupt dielectric discontinuities between bulk and ambient for main semiconductor materials, which include two key steps of chemical etch-polishing and stripping procedures. Their results are summarized in Table. 2.1 for reference.

2.3.2 The ellipsometric formula of multilayer

So far we have considered the surface of sample to be free from any overlayer. As mentioned in the above section, in the actual sample there usually exists an interface layer between the intrinsic material and ambient, such as oxide layer and rough layer etc. Therefore, it is necessary that the general formula of ellipsometry with multilayers be developed.

The formula of one-layer can be simply derived and the more general formula of multilayer can be obtained by repetitiously using the formula of one-layer. The physical model of the

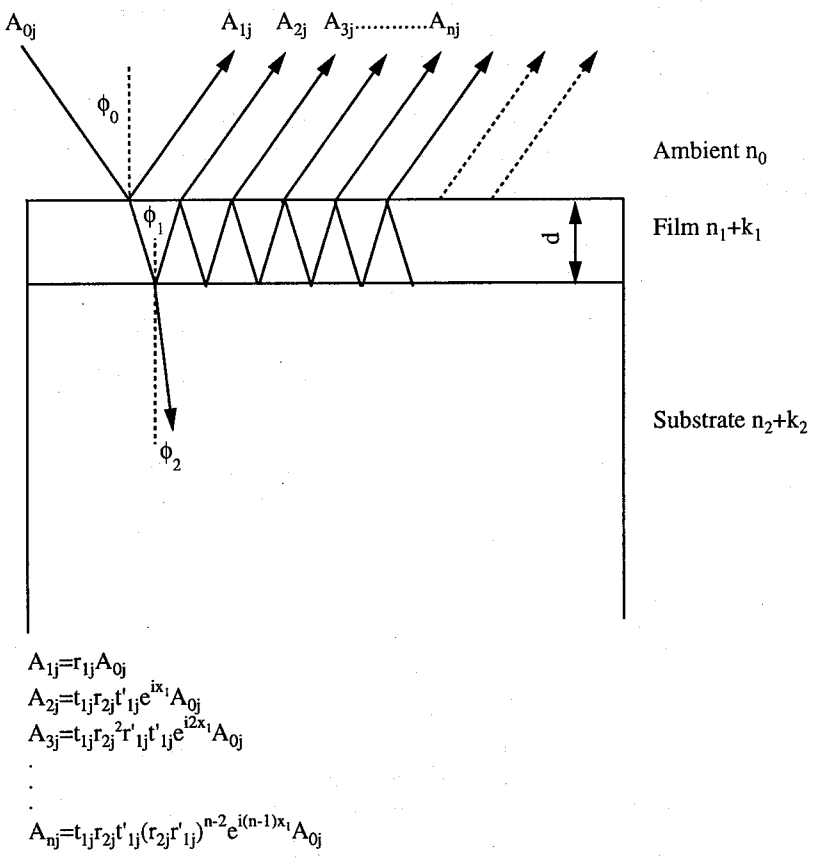

Figure 2.7: The three-phase model of ellipsometry

materials under ellipsometric investigation is based on the following assumptions.

1. The materials forming the system are optically isotropic and homogeneous.

2. All boundaries of system are ideally flat, smooth and infinitely thin.

3. The ambient is a non-absorbing media characterized by a real refractive index n_0.

Complete optical analysis of the one-layer system shown in Fig. 2.7 is performed when the values of three optical parameters, i.e. the complex refractive indices of substrate and the film, and the thickness d_1 of the film are determined (the value of n_0 is assumed to be known). The total reflective amplitude (A_j) from the two surfaces is,

$$A_j = \hat{r}_{1j}A_{0j} + \hat{t}_{1j}\hat{r}_{2j}\hat{t}'_{1j}e^{ix_1}A_{0j} + \hat{t}_{1j}\hat{r}^2_{2j}\hat{r}'_{1j}\hat{t}'_{1j}e^{i2x_1}A_{0j} +$$

$$\cdots + \hat{t}_{1j}\hat{r}_{2j}\hat{t}'_{1j}\left(\hat{r}_{2j}\hat{r}'_{1j}\right)^{n-1} e^{i(n-1)x_1} A_{0j} \tag{2.21}$$

where $\hat{r}_1$ ($\hat{r}'_1$), $\hat{t}_1$ $\left(\hat{t}'_1\right)$ are the reflection and transmission on the outer boundary of the film surface, respectively, and $\hat{r}_2$ ($\hat{r}'_2$), $\hat{t}_2$ $\left(\hat{t}'_2\right)$ are the reflection and transmission on the inner boundary of the film surface, respectively, x_1 is the difference of phase. The relations of $\hat{r}_{1j} = -\hat{r}'_{1j}$ and $1 = \hat{r}^2_{1j} + \hat{t}_{1j}\hat{t}'_{1j}$ come into existence. The reflection ($\hat{r}_j = \hat{A}_j/A_{0j}$) is given by

$$\begin{aligned}
\hat{r}_j &= \hat{r}_{1j} + \hat{t}_{1j}\hat{t}'_{1j}\hat{r}_{2j}e^{ix_1}\left(1 + \hat{r}_{2j}\hat{r}'_{1j} + \cdots + \left(\hat{r}_{2j}\hat{r}'\right)^{n-2} e^{i(n-2)x_1}\right) \\
&= \hat{r}_{1j} + \hat{t}_{1j}\hat{t}'_{1j}\hat{r}_{2j}e^{ix_1}\frac{1 - \left(\hat{r}_{2j}\hat{r}'_{1j}e^{ix_1}\right)^{n-1}}{1 - \hat{r}_{2j}\hat{r}'_{1j}e^{ix_1}} \\
&= \hat{r}_{1j} + \frac{\hat{t}_{1j}\hat{t}'_{1j}\hat{r}_{2j}e^{ix_1}}{1 + \hat{r}_{2j}\hat{r}_{1j}e^{ix_1}} \\
&= \frac{\hat{r}_{1j} + \left(\hat{r}^2_{1j} + \hat{t}_{1j}\hat{t}'_{1j}\right)\hat{r}_{2j}e^{ix_1}}{1 + \hat{r}_{2j}\hat{r}_{1j}e^{ix_1}} \\
&= \frac{\hat{r}_{1j} + \hat{r}_{2j}e^{ix_1}}{1 + \hat{r}_{2j}\hat{r}_{1j}e^{ix_1}}, \qquad\qquad j = p, s
\end{aligned} \tag{2.22}$$

The reflection of each surface are given by

$$\begin{aligned}
&\hat{r}_{1p} = \frac{\hat{n}_1\cos\phi_0 - n_0\cos\hat{\phi}_1}{\hat{n}_1\cos\phi_0 + n_0\cos\hat{\phi}_1}, \quad \hat{r}_{1s} = \frac{n_0\cos\phi_0 - \hat{n}_1\cos\hat{\phi}_1}{n_0\cos\phi_0 + \hat{n}_1\cos\hat{\phi}_1}, \\
&\hat{r}_{2p} = \frac{\hat{n}_2\cos\hat{\phi}_1 - \hat{n}_1\cos\hat{\phi}_2}{\hat{n}_2\cos\hat{\phi}_1 + \hat{n}_1\cos\hat{\phi}_2}, \quad \hat{r}_{2s} = \frac{\hat{n}_1\cos\hat{\phi}_1 - \hat{n}_2\cos\hat{\phi}_2}{\hat{n}_1\cos\hat{\phi}_1 + \hat{n}_2\cos\hat{\phi}_2}, \\
&x_1 = (4\pi/\lambda)\,\hat{n}_1 d_1\cos\hat{\phi}_1, \quad \cos\hat{\phi}_1 = (1/\hat{n}_1)\sqrt{\hat{n}^2_1 - n^2_0\sin^2\phi_0}, \\
&\cos\hat{\phi}_2 = (1/\hat{n}_2)\sqrt{\hat{n}^2_2 - n^2_0\sin^2\phi_0}.
\end{aligned} \tag{2.23}$$

The ellipsometric parameters Δ and Ψ are given by

$$\tan\Psi e^{i\Delta} = \hat{R}_p/\hat{R}_s, \tag{2.24}$$

They are dependent on the following quantities: $\hat{n}_1$, d_1, $\hat{n}_2$, n_0, ϕ_0 and λ, where ϕ_0 and λ are the angle of incidence of the light on the upper boundary of the surface film and the wavelength of the incident light, respectively. Thus, it is impossible that three unknown parameters of a film n_1, k_1 and d_1 for one-layer system and more number of unknown parameters for a multilayer system be directly determined by using two measurable values

of ellipsometric parameters at a certain wavelength. However, the experimental values of the ellipsometric parameters can be interpreted by means of a least-squares method (LSM). According to this method it is necessary to carry out a minimalization of the unbiased estimator (δ):

$$\delta^2 = \frac{1}{N-p-1}\left(\sum_{i=1}^{N}\left|\rho_i^{exp\,t} - \rho_i^{calc}\right|^2\right) \tag{2.25}$$

where N denotes the number of the experimental points and p the number of the individual and wavelength-independent parameters.

The values of the unbiased estimator δ is an indication of how close the fitting procedure matches the experimental data. Various sources may contribute to ensure that the estimator δ does not approach zero as the model is finely tuned toward the best fit, such as the experimental error, the modeling procedure, the use of inappropriate reference dielectric functions, or the possible complications in the sample microstructure that cannot be easily modeled.

2.4 Modeling of spectroscopic ellipsometric (SE) data (Levenberg-Marquardt Method)

To minimize χ_u^2 in Eq. 2.2 to get the parameters $\mathbf{z}$, one must make the gradient of χ_u^2 with respect to the parameters $\mathbf{z}$ reaching zero at the χ_u^2 minimum. We expect $\tan\Psi(\mathbf{z})$ and $\cos\Delta(\mathbf{z})$ functions to be well approximated by a line form, which can be written as

$$\begin{aligned}
\tan\Psi_{calc}(\lambda,\mathbf{z}) &= \tan\Psi_{calc}(\lambda,\mathbf{z}_{cur}) \\
&+ \left(\frac{\partial\tan\Psi_{calc}(\lambda_i,\mathbf{z}_{cur})}{\partial z_1} \quad \frac{\partial\tan\Psi_{calc}(\lambda_i,\mathbf{z}_{cur})}{\partial z_2} \quad \ldots\right)\begin{pmatrix}\delta z_1\\ \delta z_2\\ \vdots\end{pmatrix} \\
&= \tan\Psi_{calc}(\lambda,\mathbf{z}_{cur}) + \beta_1\cdot\delta\mathbf{z} \\
\cos\Delta_{calc}(\lambda,\mathbf{z}) &= \cos\Delta_{cal}(\lambda,\mathbf{z}_{cur}) \\
&+ \left(\frac{\partial\cos\Delta_{calc}(\lambda_i,\mathbf{z}_{cur})}{\partial z_1} \quad \frac{\partial\cos\Delta_{calc}(\lambda_i,\mathbf{z}_{cur})}{\partial z_2} \quad \ldots\right)\begin{pmatrix}\delta z_1\\ \delta z_2\\ \vdots\end{pmatrix} \\
&= \cos\Delta_{cal}(\lambda,\mathbf{z}_{cur}) + \beta_2\cdot\delta\mathbf{z}
\end{aligned} \tag{2.26}$$

where $\mathbf{z}_{cur}$ are the current trial parameters and $\delta\mathbf{z}$ are their increments. In this way, the gradient of χ^2_u with respect to the increments (δ z) has components

$$\begin{aligned}\frac{\partial\chi^2_u}{\partial\delta z_k} = & - \frac{2}{n-p-1}\sum_{i=1}^{n}[(\tan\Psi_{\exp}(\lambda_i) - \tan\Psi_{calc}(\lambda_i,\mathbf{z}_{cur}) - \beta_1\cdot\delta\mathbf{z})\,\beta_{1k} \\ & + (\cos\Delta_{\exp}(\lambda_i) - \cos\Delta_{calc}(\lambda_i,\mathbf{z}_{cur}) - \beta_2\cdot\delta\mathbf{z})\,\beta_{2k}] \end{aligned} \tag{2.27}$$

The gradient of χ^2_u is zero with the increments of δ z at the minimum. From this condition it can been obtained that

$$\begin{aligned}&\sum_{l=1}^{M}\left[\sum_{i=1}^{n}(\beta_{1l}\beta_{1k}+\beta_{2l}\beta_{2k})\right]\delta z_l \\ &= \sum_{i=1}^{n}[(\tan\Psi_{\exp}(\lambda_i) - \tan\Psi_{calc}(\lambda_i,\mathbf{z}_{cur}))\,\beta_{1k} + (\cos\Delta_{\exp}(\lambda_i) - \cos\Delta_{calc}(\lambda_i,\mathbf{z}_{cur}))\,\beta_{2k}].\end{aligned}$$

Let

$$\begin{aligned}\alpha_{lk} &= \sum_{i=1}^{n}(\beta_{1l}\beta_{1k}+\beta_{2l}\beta_{2k}) \\ &= \sum_{i=1}^{n}\left[\frac{\partial\tan\Psi(\lambda_i,\mathbf{z}_{cur})}{\partial z_l}\frac{\partial\tan\Psi(\lambda_i,\mathbf{z}_{cur})}{\partial z_k} + \frac{\partial\cos\Delta(\lambda_i,\mathbf{z}_{cur})}{\partial z_l}\frac{\partial\cos\Delta(\lambda_i,\mathbf{z}_{cur})}{\partial z_k}\right]\end{aligned} \tag{2.28}$$

and

$$\begin{aligned}\beta_k = & \sum_{i=1}^{n}\left[(\tan\Psi_{\exp}(\lambda_i) - \tan\Psi_{calc}(\lambda_i,\mathbf{z}_{cur}))\frac{\partial\tan\Psi_{calc}(\lambda_i,z_{cur})}{\partial z_k}\right. \\ & \left. + (\cos\Delta_{\exp}(\lambda_i) - \cos\Delta_{calc}(\lambda_i,\mathbf{z}_{cur}))\frac{\partial\cos\Delta_{calc}(\lambda_i,z_{cur})}{\partial z_k}\right]\end{aligned} \tag{2.29}$$

The set of linear equations can be written as

$$\sum_{l=1}^{M}\alpha_{lk}\delta z_l = \beta_k \tag{2.30}$$

This set is solved for the increments δz_l that, added to the current approximation, give the next approximation. Minor (or even major) fiddling with [α] has no effect at all on what final set of parameters z is reached, but only affects the iterative route that is taken in getting there. The condition at the χ^2_u minimum, that β_k=0 for all k, is independent of how [α] is defined.

In Eq. 2.30, δz and β are an M-vector and α is an M×M matrix. Scan the components of [α] and find that there is only one obvious quantity with these dimensions, and that is

$1/\alpha_{kk}$, the reciprocal of the diagonal element. So that must set the scale of the constant. But that scale might itself be too big. So let's divide the constant by some (nondimensional) fudge factor λ, with the possibility of setting $\lambda \ll 1$ to cut down the step. In other words, replace equation 2.30 by

$$\lambda \alpha_{ll} \delta z_l = \beta_l \tag{2.31}$$

It is necessary that α_{ll} be positive, but this is guaranteed by definition 2.28 - another reason for adoption of that equation.

Eq. 2.31 and 2.30 can be combined if we define a new matrix α' by the following prescription

$$\begin{aligned} \alpha'_{jj} &\equiv \alpha_{jj}(1+\lambda) \\ \alpha'_{jk} &\equiv \alpha_{jk} \end{aligned} \tag{2.32}$$

and then replace both 2.31 and 2.30 by

$$\sum_{l=1}^{M} \alpha'_{lk} \delta z_l = \beta_k \tag{2.33}$$

When λ is very large, the matrix α' is forced into being *diagonallydominant*, so equation 2.33 goes over to be identical to 2.31. On the other hand, as λ approaches to zero, equation 2.33 goes to 2.30.

Given an initial guess for the set of fitted parameters $\mathbf{z}$, the recommended Levenberg-Marquardt recipe is as follows:

- Compute $\chi^2_u(\mathbf{v})$.
- Pick a modest value for λ, say λ=0.001.
- (†) Solve the linear equations (2.33) for $\delta\mathbf{v}$ and evalute $\chi^2_u(\mathbf{v}+\delta\mathbf{v})$.
- If $\chi^2_u(\mathbf{v}+\delta\mathbf{v}) > \chi^2_u(\mathbf{v})$, *increase*$\lambda$ by a factor of 10 (or any other substantial factor) and go back to (†).
- if If $\chi^2_u(\mathbf{v}+\delta\mathbf{v}) < \chi^2_u(\mathbf{v})$, *decrease*$\lambda$ by a factor of 10, updata the trial solution $\mathbf{v} \leftarrow \mathbf{v}+\delta\mathbf{v}$, and go to back to (†).

Also necessary is a condition for stopping. Iterating to convergence (to machine accuracy or to the roundoff limit) is generally wasteful and unnecessary since the minimum is at best only a statistical estimate of the parameters **v**.

Confidence limits on estimated model parameters

Table 2.2: $\Delta\chi^2_u$ as a function of confidence level and degrees of freedom.

	ν					
p	1	2	3	4	5	6
68.3%	1.00	2.30	3.53	4.72	5.89	7.04
90%	2.71	4.61	6.25	7.78	9.24	10.6
95.4%	4.00	6.17	8.02	9.70	11.3	12.8
99%	6.63	9.21	11.3	13.3	15.1	16.8
99.73%	9.00	11.8	14.2	16.3	18.2	20.1
99.99%	15.1	18.4	21.1	23.5	25.7	27.8

The standard errors of parameters can be estimated by following procedure:

- Let ν be the number of fitted parameters whose joint confidence region you wish to display, $\nu \leq M$. Call these parameters the "parameters of interest".
- Let p be the confidence limit desired, e.g. p=0.68 or p=0.95.
- Find Δ (i.e. $\Delta\chi^2_u$) such that the probability of a chi-square variable with ν degrees of freedom being less than Δ is p. For some useful values of p and ν, Δ is given in the table 2.2. For other values, the routine **gammq** and simple root-finding routine (e.g. bisection) can be used to find Δ such that **gammq**($\nu/2$, $\Delta/2$)=1-p.
- Taken the M×M covariance matrix [C]=$[\alpha]^{-1}$ of the chi-square fit.
- The standard errors of parameters (δz_k) is given by

$$\delta z_k = \pm\sqrt{\Delta\chi^2_u}\sqrt{C_{kk}}$$

2.5 The main analysis models for semiconductor

2.5.1 A modified harmonic oscillator approximation scheme for the dielectric constants of semiconductor

Theoretical models

The optical dielectric function of a semiconductor with Lorentzian line broadening is given by the equation[21)]

$$\varepsilon(\omega) = 1 - \frac{8\pi e^2\hbar^2}{m^2}\sum_{cv}\int dE \frac{W_{cv}(E)}{E^2}\left[\frac{1}{\hbar\omega - E + i\Gamma(E)} - \frac{1}{\hbar\omega + E + i\Gamma(E)}\right], \quad (2.34)$$

where $W_{cv}(E)=|P_{cv}(E)|^2 J_{cv}(E)$.

c and v stand for the conduction and the valence band, respectively, $E\equiv E_{cv}(k)$ is the energy difference between a pair of bands in k space, $J_{cv}(E)$ is the joint density of states between a pair of bands, and $P_{cv}(E)$ is the weighted-average matrix element of the momentum operator. Since $P_{cv}(E)$ is a slowly varying function of E, the analytical structure of $J_{cv}(E)$ is only considered. In general, in three dimensions, $J_{cv}(E)$ has four possible types of critical points M_0, ..., M_3. Each type has a square-root singularity. The shapes of M_0, ..., M_3 are shown schematically in Fig. 2.8. The $W_{cv}(E)$ in the vicinity of critical points of type M_0,..., M_3 is written as,

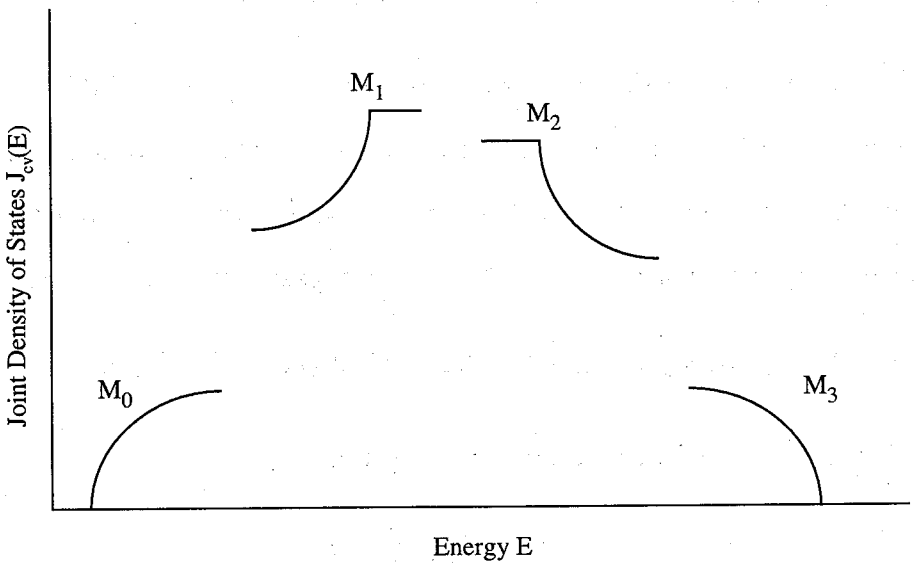

Figure 2.8: Schematic drawings of $J_{cv}(E)$ in the vicinity of critical points.

$$M_0:\ W_{cv}(E)=\begin{cases}0 & E<E_j\\ \frac{2A'_j}{\alpha_j\sqrt{\pi}}\left(\frac{E-E_j}{\alpha_j}\right)^{1/2}\exp\left(-\frac{E-E_j}{\alpha_j}\right) & E\geq E_j\end{cases} \tag{2.35}$$

$$M_3:\ W_{cv}(E)=\begin{cases}\frac{2A'_j}{\alpha_j\sqrt{\pi}}\left(\frac{E_j-E}{\alpha_j}\right)^{1/2}\exp\left(-\frac{E_j-E}{\alpha_j}\right) & E\leq E_j\\ 0 & E>E_j\end{cases} \tag{2.36}$$

$$M_1:\ W_{cv}(E)=\begin{cases}\frac{A'_j}{4\alpha_j}exp\left(-\sqrt{\frac{E_j-E}{\alpha_j}}\right) & E<E_j\\ \frac{A'_j}{4\alpha_j} & E_j\leq E\leq E_j+2\alpha_j\\ 0 & E>E_j+2\alpha_j\end{cases} \tag{2.37}$$

$$M_2:\ W_{cv}(E)=\begin{cases}0 & E<E_j-2\alpha_j\\ \frac{A'_j}{4\alpha_j} & E_j-2\alpha_j\leq E\leq E_j\\ \frac{A'_j}{4\alpha_j}exp\left(-\sqrt{\frac{E-E_j}{\alpha_j}}\right) & E>E_j\end{cases} \tag{2.38}$$

As an example, eq. 2.37 at the critical point E_j is expanded, and obtain:

$$W_{cv}(E)=\begin{cases}\frac{A'_j}{4\alpha_j}\left(1-\sqrt{\frac{E_j-E}{\alpha_j}}\right) & E<E_j\\ \frac{A'_j}{4\alpha_j} & E_j\leq E\leq E_j+2\alpha_j\\ 0 & E>E_j+2\alpha_j\end{cases}$$

This corresponds to the "*VanHove*" singularity.[22] Therefore, above $W_{cv}(E)$'s have the physical character of a Van Hove singularity in the vicinity of a critical point, and W_{cv} approaches $A'_j * \delta(E-E_j)$ in the limit $\alpha_j \to 0$. Clearly, the substitution of a δ function into eq. 2.34 leads to the harmonic oscillator approximation. Therefore, the modified factor α_j is an important parameter which is related to the band structure.

With the substitution of $W_{cv}(E)$ into eq. 2.34, the integral in eq. 2.34 can be performed under the condition of $\alpha \ll 1$. (see Appendix A) Therefore, the contribution to $\varepsilon(\omega)$ from each critical point becomes:

$$-A_j\left(\frac{1}{\hbar\omega-E_j+i\Gamma_j}-\frac{1}{\hbar\omega+E_j+i\Gamma_j}\right)$$
$$+\frac{B_j}{E_j}\left(\frac{2\hbar\omega-3E_j+2i\Gamma_j}{(\hbar\omega-E_j+i\Gamma_j)^2}-\frac{2\hbar\omega+3E_j+2i\Gamma_j}{(\hbar\omega+E_j+i\Gamma_j)^2}\right), \tag{2.39}$$

where $A_j=(8\pi e^2\hbar^2A'_j)/(m^2E_j^2)$, $B_j=\mp(3\alpha_j/2)A_j$ correspond to M_0 and M_3, respectively, and $A_j=(8\pi e^2\hbar^2A'_j)/(m^2E_j^2)$, $B_j=\pm(5\alpha_j/2)A_j$ correspond to M_1 and M_2, respectively.

Therefore, considering the contribution to $\varepsilon(\omega)$ from only critical points, the optical dielectric function $\varepsilon(\omega)$ of a semiconductor with Lorentzian line broadening is given by

$$\varepsilon(\omega)=1+\sum_j\left(-A_j\left(\frac{1}{\hbar\omega-E_j+i\Gamma_j}-\frac{1}{\hbar\omega+E_j+i\Gamma_j}\right)\right.$$

$$+\frac{B_j}{E_j}\left(\frac{2\hbar\omega-3E_j+2i\Gamma_j}{(\hbar\omega-E_j+i\Gamma_j)^2}-\frac{2\hbar\omega+3E_j+2i\Gamma_j}{(\hbar\omega+E_j+i\Gamma_j)^2}\right)\Bigg) \tag{2.40}$$

Thus far, a new model which is mathematically simple and related to the electronic energy-band structures of the medium have been developed. It does not require us to assume the shape of the critical points beforehand. The shape of the critical points is determined by the sign of the parameter B_j.

Application to GaAs

Table 2.3: The values of CP energies and line widths of GaAs obtained by fitting spectral data with this model.

Critical point (eV)	Order of the derivative, n			
	0 and 1	2	3	Simultaneous fit
$E_0(\Gamma)$	1.4241	1.4185	1.4175	1.4204
$E_0(\Gamma)+\Delta_0(\Gamma)$	1.7601	1.7601	1.7601	1.7601
$E_1(\Lambda)$	2.9281	2.9043	2.9183	2.9232
$E_1(\Lambda)+\Delta_1(\Lambda)$	3.1676	3.1671	3.1622	3.1717
$E'_0(\Delta)$	4.4871	4.4914	4.4912	4.4912
E_2X	4.46761	4.6695	4.6710	4.6761
$E_2(\Sigma)$	4.9794	4.9790	4.9789	4.9808
$\Gamma[E_0(\Gamma)]$	0.0787	0.0705	0.0726	0.0703
$\Gamma[E_0(\Gamma)+\Delta_0(\Gamma)]$	0.0576	0.0577	0.0576	0.0576
$\Gamma[E_1(\Lambda)]$	0.0867	0.0886	0.0865	0.0891
$\Gamma[E_1(\Lambda)+\Delta_1(\Lambda)]$	0.1862	0.1366	0.1353	0.1584
$\Gamma[E'_0(\Delta)]$	0.1587	0.1527	0.1414	0.1543
$\Gamma[E_2(X)]$	0.4752	0.4298	0.4243	0.4716
$\Gamma[E_2(\Sigma)]$	0.2741	0.2758	0.2758	0.2756
rms fractional error	3.98%	14.61%	14.85%	11.14%

Because there is no critical points between $E_1+\Delta_1$ and $E'_2(\Delta)$, $W_{cv}(E)=A'_0$ is assumed

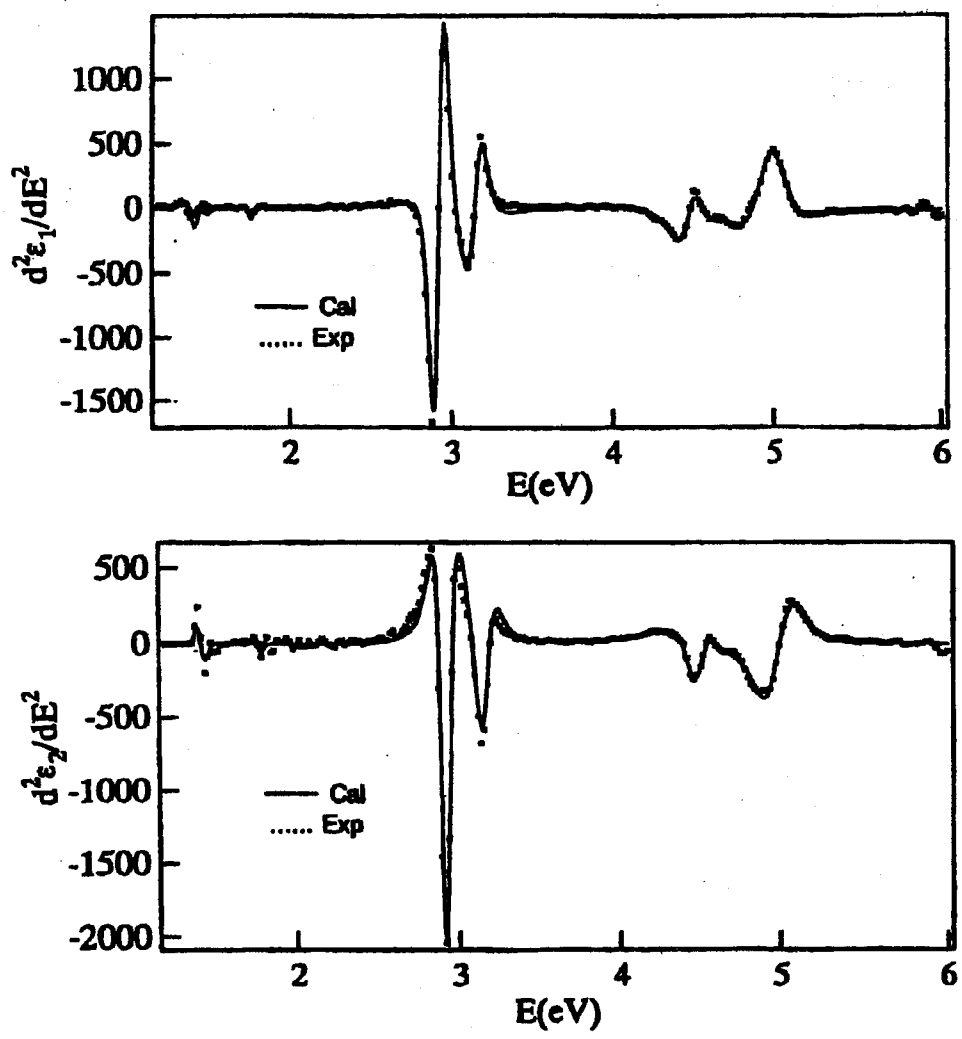

Figure 2.9: Numerically calculated second derivatives of ε_1 and ε_2 for GaAs, together with the fitting according to eq.(2.26).

in this region. Therefore, the contribution to $\varepsilon(\omega)$ from this region lead to:

$$-A_0 \int_{E_1+\Delta_1}^{E_2'(\Delta)} \frac{dE}{E^2} \left(\frac{1}{\hbar\omega - E + i(\Gamma_0 + \beta E)} - \frac{1}{\hbar\omega + E + i(\Gamma_0 + \beta E)} \right), \tag{2.41}$$

where $A_0=(8\pi e^2\hbar^2 A_0')/(m^2)$ and Γ_0 and β are constant. Therefore, the whole optical dielectric function $\varepsilon(\omega)$ is given by

$$\varepsilon(\omega) = 1 + \sum_j \left(-A_j \left(\frac{1}{\hbar\omega - E_j + i\Gamma_j} - \frac{1}{\hbar\omega + E_j + i\Gamma_j} \right) + \frac{B_j}{E_j} \left(\frac{2\hbar\omega - 3E_j + 2i\Gamma_j}{(\hbar\omega - E_j + i\Gamma_j)^2} - \frac{2\hbar\omega + 3E_j + 2i\Gamma_j}{(\hbar\omega + E_j + i\Gamma_j)^2} \right) \right)$$

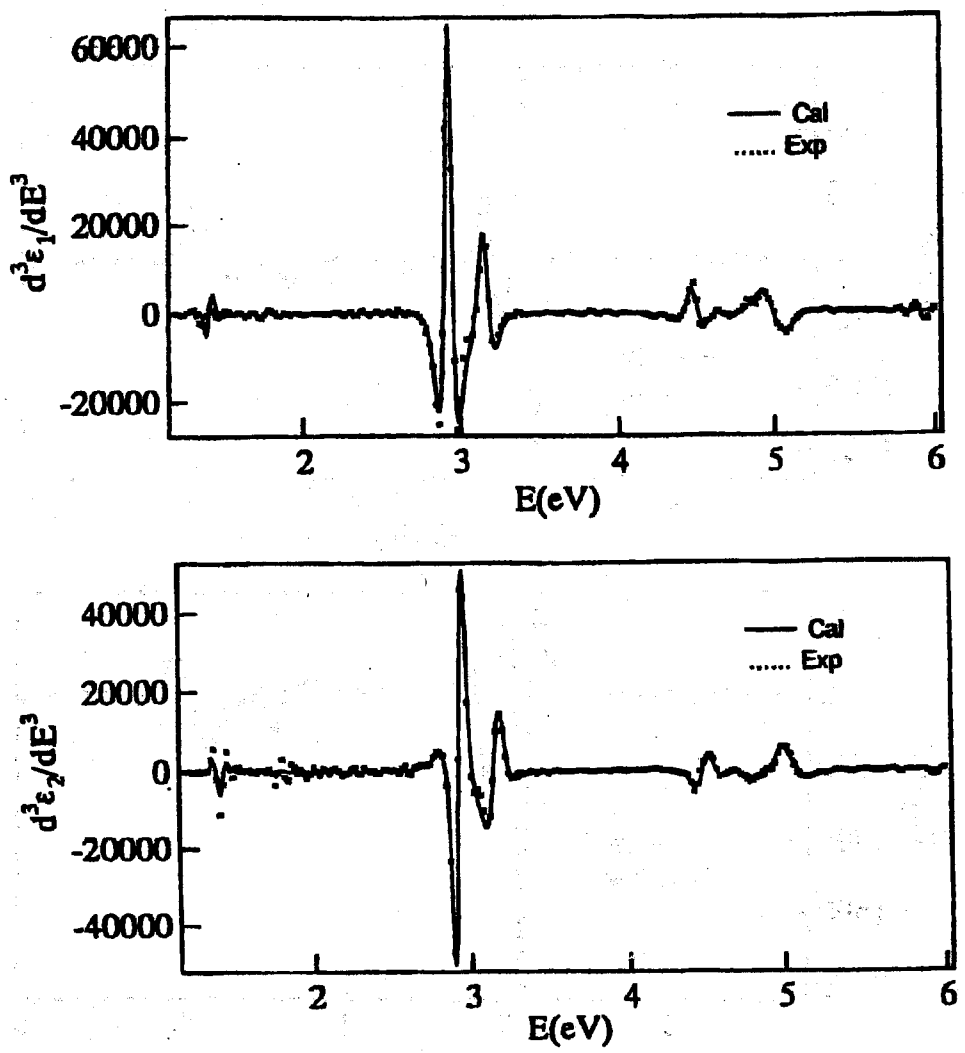

Figure 2.10: Numerically calculated third derivatives of ε_1 and ε_2 for GaAs, together with the fitting according to eq.(2.26).

$$-A_0 \int_{E_1+\Delta_1}^{E_2'(\Delta)} \frac{dE}{E^2} \left(\frac{1}{\hbar\omega - E + i(\Gamma_0 + \beta E)} - \frac{1}{\hbar\omega + E + i(\Gamma_0 + \beta E)} \right) + \sum_n^1 C_n (\hbar\omega)^n, \tag{2.42}$$

where $\sum_n^1 C_n (\hbar\omega)^n$ gives the contribution to $\varepsilon(\omega)$ from the critical points above 6 eV.

Values for both the refractive index n and extinction coefficient k between 1.2 eV and 6.0 eV are taken from the literature.[23] The values of $\varepsilon(\omega)$ are then calculated from the formula $\varepsilon(\omega) = [n(\omega) + ik(\omega)]^2$. All the spectral data for ε_1 and ε_2 are reorganized in

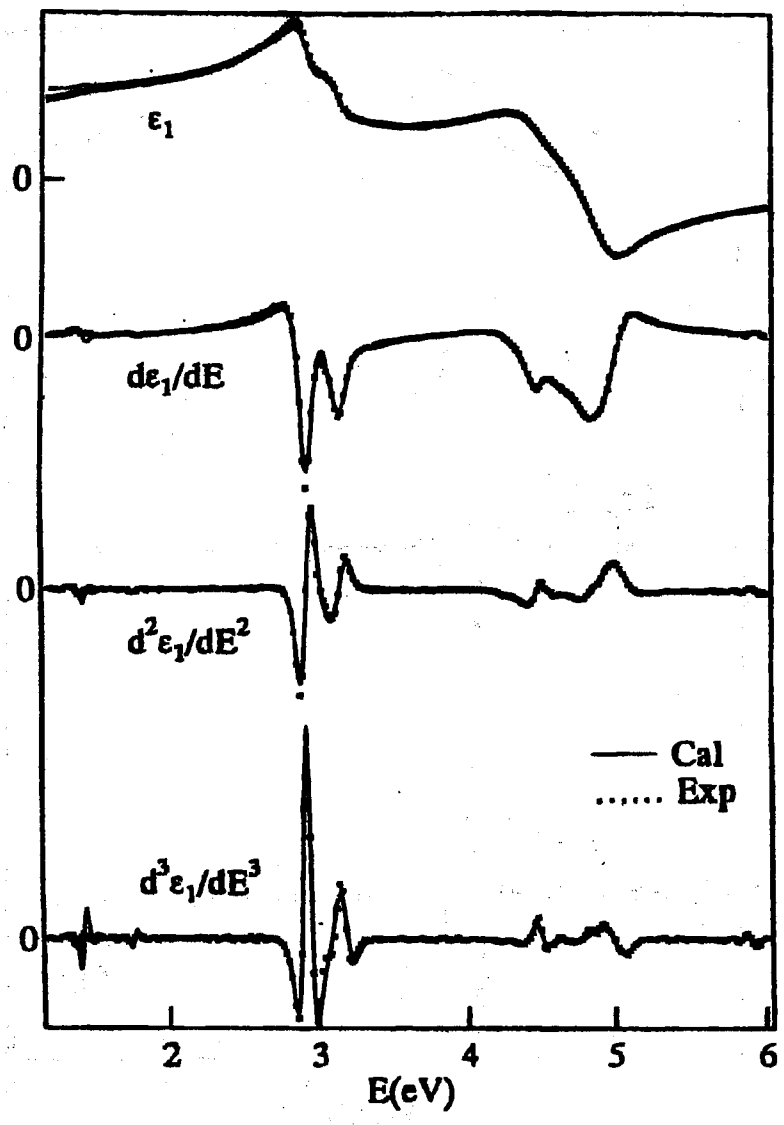

Figure 2.11: Simultaneous fits of model to $\varepsilon_1(\omega)$ for GaAs and its first three numerical deivatives.

steps of 20 meV, with use of the polynomial method where interpolation is need. The derivative spectra are obtained by numerical differentiation with cubic spline fitting routines. The simultaneous fits with model to the real and imaginary parts of the experimental $(d^2\varepsilon)/(dE^2)$, $(d^3\varepsilon)/(dE^3)$ for GaAs are shown in Figs. 2.9 and Figs. 2.10 respectively. The solid line is obtained from eq. 2.40. The parameters of the fits are listed in Table 2.3. σ is the root-mean-square (rms) fractional error, defined by Kim et al. Only seven critical points and use 28 parameters are included in this fitting. The values of critical points E_j

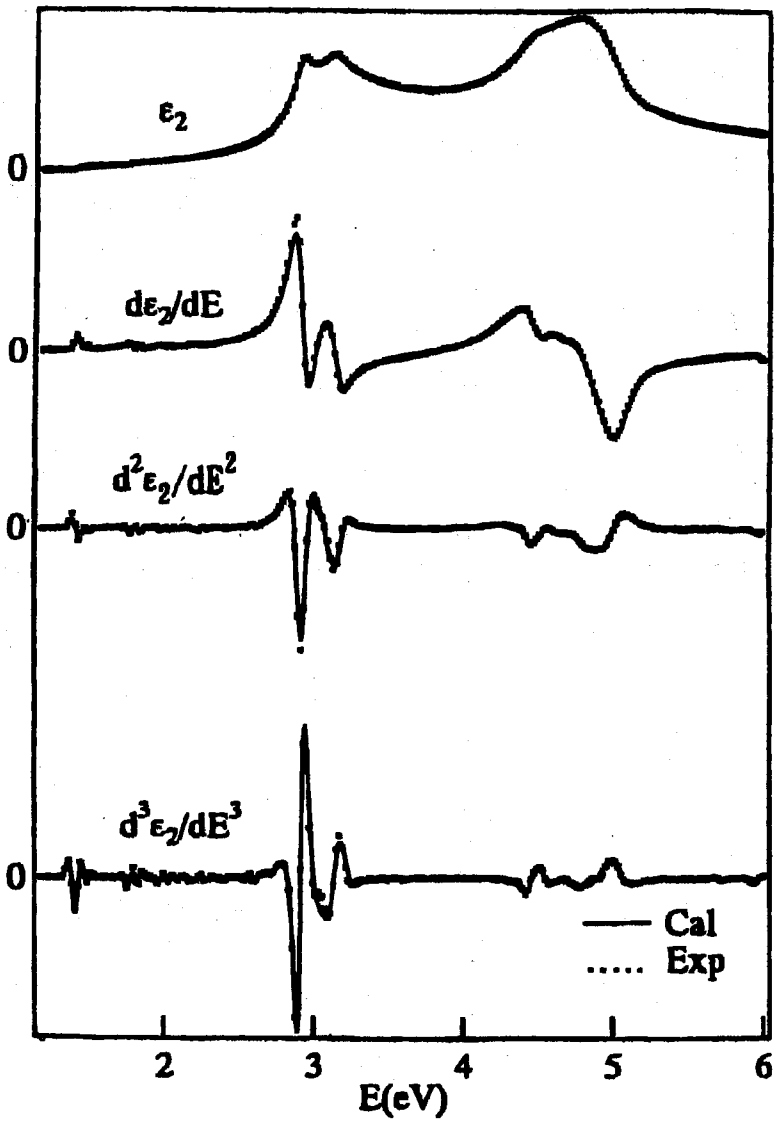

Figure 2.12: Simultaneous fits of model to $\varepsilon_2(\omega)$ for GaAs and its first three numerical deivatives.

obtained by the fitting are in good agreement with those determined by Kim et al.. Like the harmonic oscillator approximation, the values of line widths Γ_j in present model are more than twice the values of Γ_j which were found in the model of Kim et al..

Using the method described in ref. 21, the simultaneous fitting with eq. 2.42 to $\varepsilon_2(\omega)$ and its first three numerical derivatives with respect to photon energy is performed. In Fig. 2.11 and 2.12 the simultaneous fits to $\varepsilon_1(\omega)$ and $\varepsilon_2(\omega)$ and their first three numerical derivatives with respect to photon energy are shown. The solid line is obtained from eq. 2.42. Only

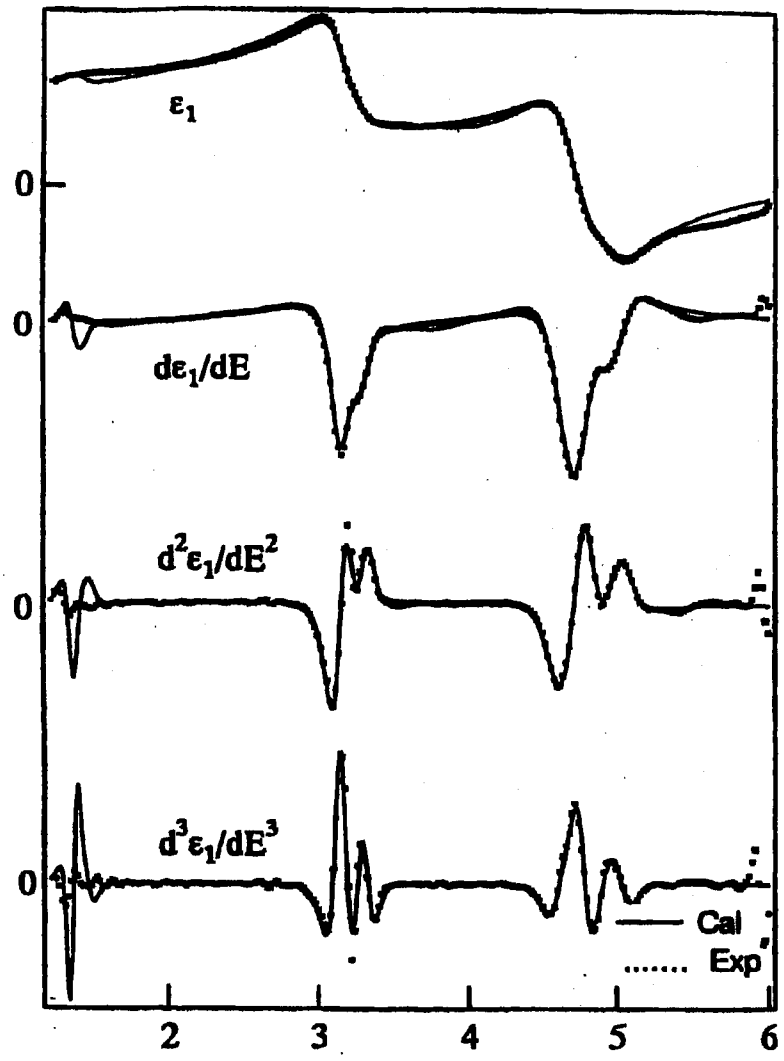

Figure 2.13: Simultaneous fits of model to $\varepsilon_1(\omega)$ for InP and its first three numerical deivatives.

32 free parameters are used in this fitting, which yielded the excellent simultaneous fits to real and imaginary parts of the optical dielectric function. The parameters of the fits are also listed in Table 2.3. The rms fractional error σ is 11.2%, which value of σ is smaller than that obtained using Kim et al's model (13.7%).

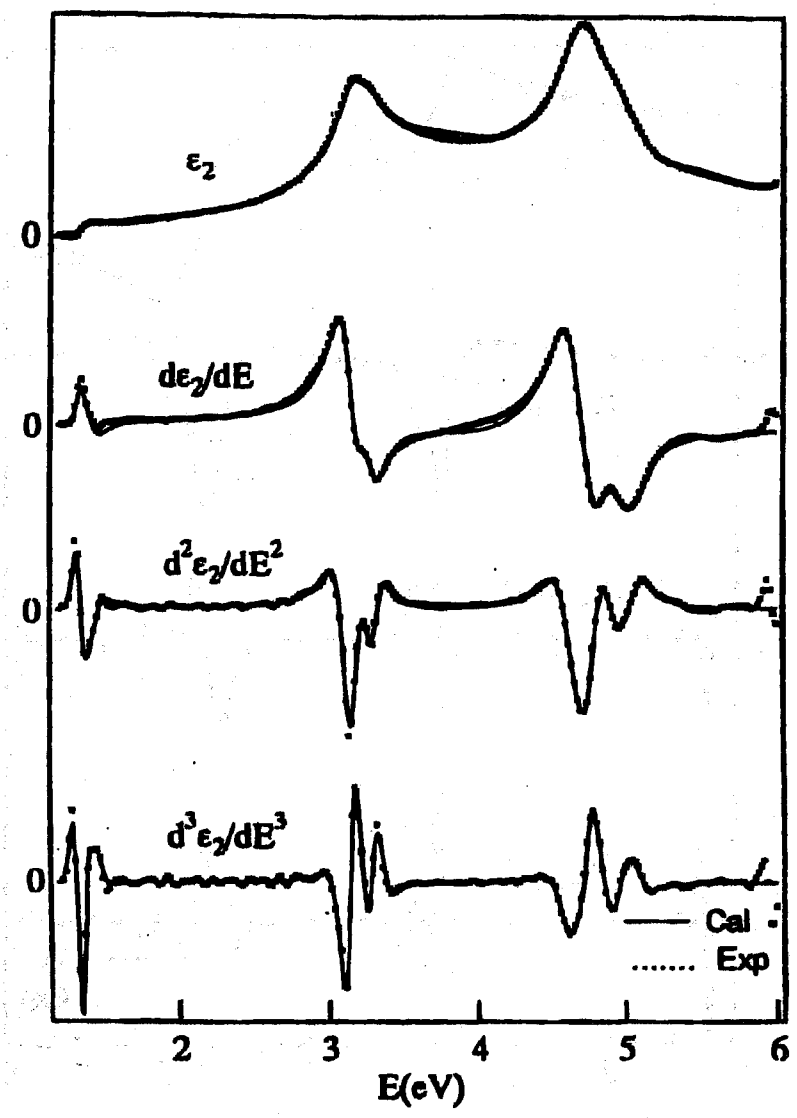

Figure 2.14: Simultaneous fits of model to $\varepsilon_2(\omega)$ for InP and its first three numerical deivatives.

Application to InP

Like GaAs, InP is a direct-gap semiconductor. As seen in Figs. 2.13 and 2.14, it is clear that there are two peaks of E_1 (3.16 eV) and $E_1+\Delta_1$ (3.31 eV) from the numerical derivatives of the dielectric function with respect to photon energy. Therefore, seven critical points were used to fit the second and the third numerical derivatives of the dielectric function with respect to photon energy, and eq. 2.42 with 32 free parameters is used for simultaneous fitting of $\varepsilon_2(\omega)$ and its first three numerical derivatives with respect to photon

Table 2.4: The values of CP energies and line widths of InP and GaP obtained by fitting spectral data its first three numerical derivatives with this model.

Critical point (eV)	Simultaneous fit	
	InP	GaP
$E_0(\Gamma)$	1.3552	2.744
$E_0(\Gamma) + \Delta_0(\Gamma)$	1.4387	2.8186
$E_1(\Lambda)$	3.1633	3.6759
$E_1(\Lambda) + \Delta_1(\Lambda)$	3.3070	
$E'_0(\Delta)$	4.6482	4.7899
E_2X	4.7425	5.2024
$E_2(\Sigma)$	5.0100	5.2231
$\Gamma[E_0(\Gamma)]$	0.0956	0.1144
$\Gamma[E_0(\Gamma) + \Delta_0(\Gamma)]$	0.1000	0.0872
$\Gamma[E_1(\Lambda)]$	0.1413	0.1291
$\Gamma[E_1(\Lambda) + \Delta_1(\Lambda)]$	0.1456	
$\Gamma[E'_0(\Delta)]$	0.2225	0.2244
$\Gamma[E_2(X)]$	0.1361	0.3306
$\Gamma[E_2(\Sigma)]$	0.2424	0.1424
rms fractional error	14.7%	5.86%

energy. A comparison of model with the experimental data for InP[23,24] and the first three numerical derivatives of those with respect to photon energy is shown in Figs. 2.13 and 2.14. The parameters of the fits are listed in Table 2.4. The model (solid line) shows an excellent agreement with the experimental data for InP and the first three numerical derivatives of those with respect to photon energy over the entire range of photon energies. The values of critical points E_j obtained by the fitting are in good agreement with those determined using the standard critical-point parabolic-band (CPPB) model. As in the case of GaAs, the values of line widths Γ_j in this model are more than twice those found using the CPPB.[25]

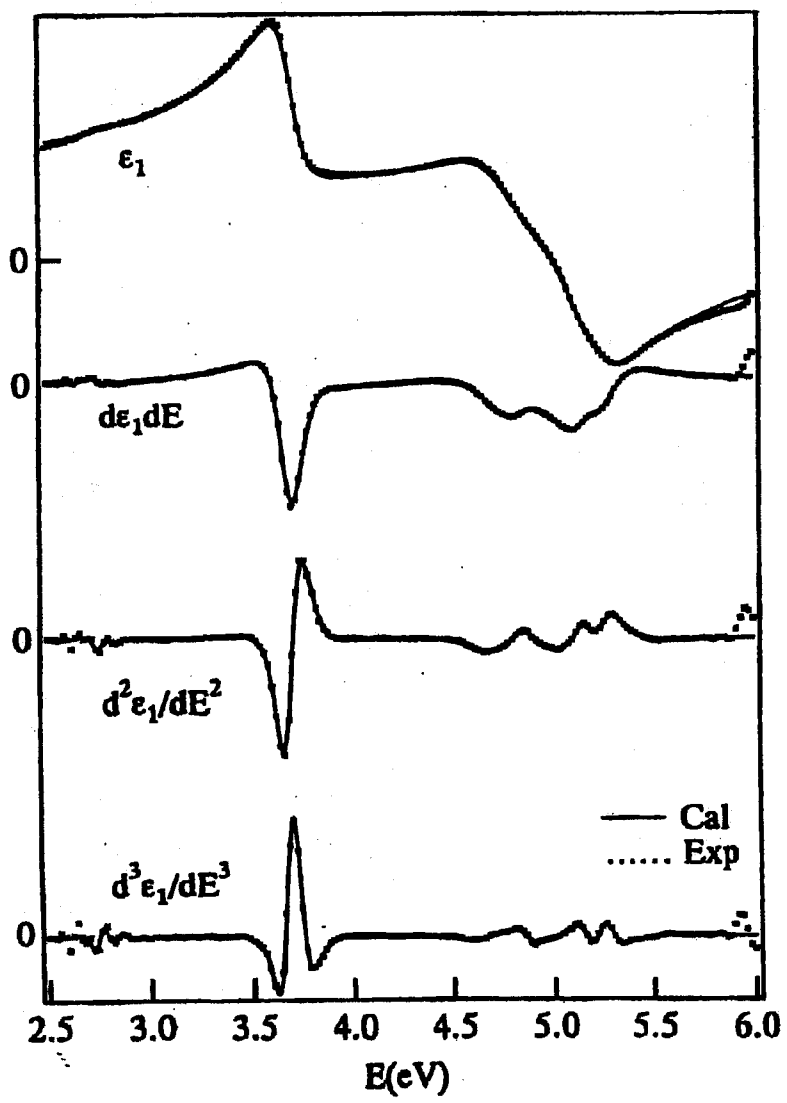

Figure 2.15: Simultaneous fits of model to $\varepsilon_1(\omega)$ for GaP and its first three numerical deivatives.

Application to GaP

The GaP crystal is known to be a typical indirect-gap material. The spin-orbit splitting energy Δ_1 in this material is rather small (<0.1 eV) and can be neglected here. Therefore, six critical points are used to fit the second and third numerical derivatives of the dielectric function with respect to photon energy, and eq. 2.42 with 30 free parameters is used to obtain simultaneous fits to $\varepsilon_2(\omega)$[23,24] and its first three numerical derivatives with respect to photon energy. Figs. 2.15 and 2.16 show the simultaneous fits with this model (solid

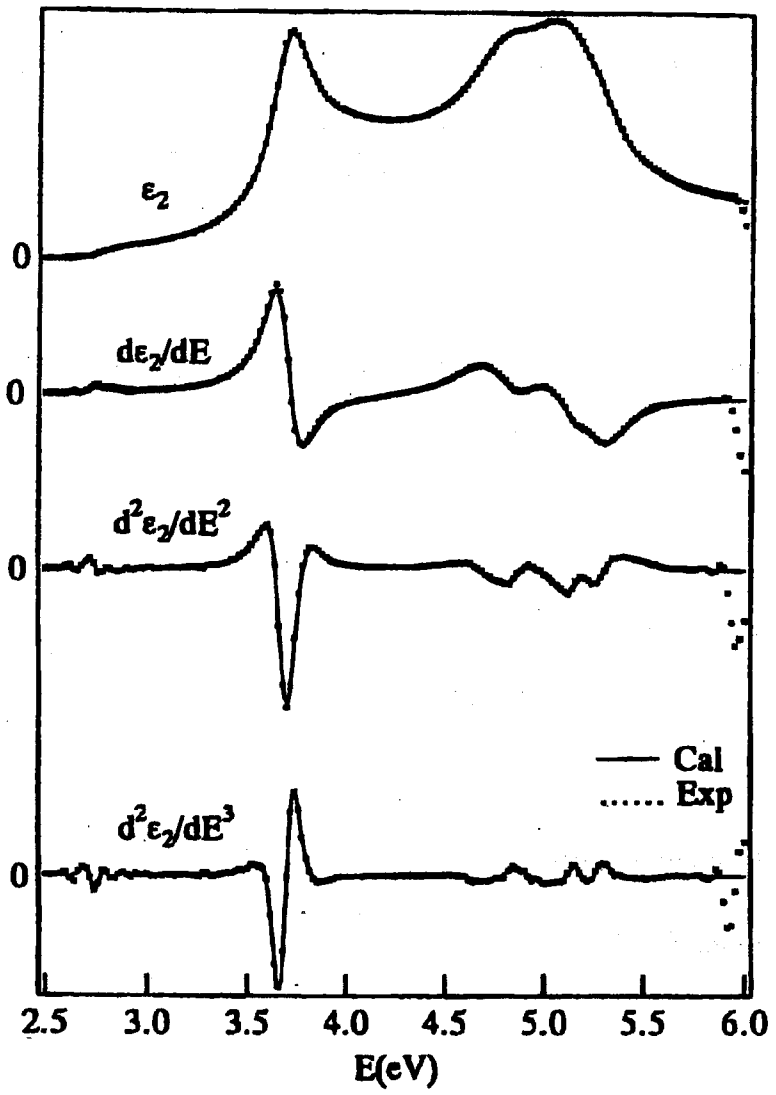

Figure 2.16: Simultaneous fits of model to $\varepsilon_2(\omega)$ for GaP and its first three numerical deivatives.

line) to the experimental ε spectrum of GaP and the first three numerical derivatives of those with respect to photon energy. The parameters of the fits are listed in Table 2.4. Unlike those of GaAs and InP, the E_1 critical-point structure is M_2-style. The value of E_1 is somewhat larger than the value obtained using the standard critical-point model, because it is assumed that the E_1 critical-point structure is M_1-style in the standard critical-point model.[15] As in the case of GaAs and InP, the theoretical model gives good agreement with the experimental data.

2.5.2 Other models for the dielectric function of semiconductor

Harmonic oscillator approximate (HOA)

In the harmonic oscillator model of Erman et al.,[26] $\varepsilon(\omega)$ is given by

$$\varepsilon(\omega) = 1 - \sum_{k=1}^{n} A_k \left(\frac{1}{\hbar\omega - E_k + i\Gamma_k} - \frac{1}{\hbar\omega + E_k + i\Gamma_k} \right), \tag{2.43}$$

where E_k is the energy of a harmonic oscillator and Γ_k is its linewidth. Equation 2.43 is much simple than Eq. 2.34 by a sum of Lorentzians. In principle, each single transition from a lower band to higher band could be represented by a harmonic oscillator, but in practice the minimum possible number of oscillators is used to represent the dielectric function. This model fails to describe $\varepsilon(\omega)$ below or around the band edge at E_0 because $\varepsilon_2(\omega)$ has a broadened square-root singularity at the band edge with little background, whereas the HOA model yields only a sum of Lorentzian peaks for $\varepsilon_2(\omega)$. The HOA energies E_k are not simply related to the CP energies E_j, this model is not simply related to the band structure.

The standard critical-point parabolic-band (CPPB) model

The CPPB model[27,28] gives an accurate representation of the derivatives of $\varepsilon(\omega)$ of order higher than first order, because the critical point structure is greatly enhanced in those derivatives. Thus its use enables one to determine the CP energies and line widths quite accurately. However, this model gives only a very poor representation of dielectric function itself and is not suitable for the description of the dielectric function or its first derivative with respect to photon energy, temperature or pressure.

Within a CP model, $\varepsilon(\omega)$ in Eq. 2.34 usually is given by the approximate formula

$$\varepsilon(\omega) = 1 - \frac{8\pi e^2}{m^2\omega^2} \sum_j P_j^2 \int dE \frac{J_j(E)}{\hbar\omega - E + i\Gamma_j}. \tag{2.44}$$

Here, the sum over c and v in Eq. 2.34 is replaced by a sum the critical points j, which implicitly contains a sum over c and v. In this model $P_{cv}(E)$ in Eq. 2.34 is considered to be constant P_j. The second term in the second set of large parentheses in Eq. 2.34, being much smaller in magnitude than the first term near any critical point, is usually

neglected. Finally, the factor E^{-2} in Eq. 2.34 is replaced by $(\hbar\omega)^{-2}$. This is justified only if the spectral range of the contribution of each CP is limited to the region $|\hbar\omega - E_j| \ll E_j$ near the CP. This approximation leads to a serious analytic error, a divergence in $\varepsilon(\omega)$ as $\omega \rightarrow 0$, as well as quantitative errors. Also, note that the usual neglect of the second term in the second set of large parentheses in Eq. 2.34, although it is not so serious as the previous approximation, does prevent $\varepsilon_2(\omega)$ from going to zero as $\omega \rightarrow 0$, as it should.

In the immediate vicinity of any three-dimensional (3D) CP of type M_j, $E_{cv}(\mathbf{k})$ is a parabolic function of $\mathbf{k}$. Thus, each 3D CP is characterized by a square-root singularity, the M_0 and M_2 two-dimensional (2D) critical points are characterized by a discontinuity in $J_{cv}(E)$, and each one-dimensional CP is characterized by an inverse square-root singularity. Excluding the only remaining type of CP, the 2D M_1 CP, which does not occur, the derivatives of $\varepsilon(\omega)$ can be represented within the CPPB approximation by the equation

$$\frac{d^n}{d\omega^n}\left[\omega^2\varepsilon(\omega)\right] = \sum_j C_j \frac{e^{i\theta_j}}{(\hbar\omega - E_j + i\Gamma_j)^{1+n-0.5d_j}}, \tag{2.45}$$

where C_j is a constant, and d_j is the dimensionality of the CP. In the neglect of many-body effects, the phase angle θ_j is given by the equation[29)]

$$\theta_j = \frac{\pi}{2}(j - d_j) \tag{2.46}$$

However, usually θ_j is treated as an adjustable parameter. The parametrization of value of θ_j is justified in the literature as representing the effect of excitons near the CP energy. However, this justification is at best questionable, because θ_j is found to be very near its theoretical value for the E_0 and $E_0+\Delta_0$ critical points, at which one might except excitons, but is found to be very different from the value expected theoretically for d=2 and d=3 at the E_1 and $E_1+\Delta_1$ critical points, near which one does not expect excitons.

Appendix

Substituting eq. 2.35 into eq. 2.34 lead to

$$\varepsilon(\omega) = 1 - \frac{8\pi e^2\hbar^2}{m^2}\int_{E_j}^{\infty}\frac{2A_j'}{\alpha_j\sqrt{\pi}E^2}\left(\frac{E-E_j}{\alpha_j}\right)^{1/2}\exp\left(-\frac{E-E_j}{\alpha_j}\right) * \left(\frac{1}{\hbar\omega - E + i\Gamma_j} - \frac{1}{\hbar\omega + E + i\Gamma_j}\right)dE \tag{2.47}$$

Let t=(E-E$_j$)/α_j,

$$\begin{aligned}\varepsilon(\omega) &= 1-\frac{8\pi e^2\hbar^2}{m^2}\int_0^\infty \frac{2A'_j}{\sqrt{\pi}\left(\alpha_j t+E_j\right)^2}t^{1/2}e^{-t}\left(\frac{1}{\hbar\omega-\alpha_j t-E_j+i\Gamma_j}-\frac{1}{\hbar\omega+\alpha_j t+E_j+i\Gamma_j}\right)dt \\ &= 1-\frac{16A'_j\pi e^2\hbar^2}{\sqrt{\pi}m^2}\int_0^\infty t^{1/2}e^{-t}f\left(\alpha_j,t\right)dt, \end{aligned} \tag{2.48}$$

In order to obtain a simple formula for $\varepsilon(\omega)$, the function $f(\alpha_j,t)$ is expanded into a power series of α_j, and truncate the series after the first two terms:

$$\begin{aligned} f\left(\alpha_j,t\right) = &\frac{1}{E_j^2}\left(\frac{1}{\hbar\omega-E_j+i\Gamma_j}-\frac{1}{\hbar\omega+E_j+i\Gamma_j}\right) \\ &-\frac{\alpha_j t}{E_j^3}\left(\frac{2\hbar\omega-3E_j+2i\Gamma_j}{\left(\hbar\omega-E_j+i\Gamma_j\right)^2}-\frac{2\hbar\omega+3E_j+2i\Gamma_j}{\left(\hbar\omega+E_j+i\Gamma_j\right)^2}\right), \end{aligned} \tag{2.49}$$

Substituting eq. 2.49 into eq. 2.48, the integral eq. 2.48 can be evaluated as

$$\begin{aligned} \varepsilon(\omega) = 1 &- A_j\left(\frac{1}{\hbar\omega-E_j+i\Gamma_j}-\frac{1}{\hbar\omega+E_j+i\Gamma_j}\right) \\ &+\frac{B_j}{E_j}\left(\frac{2\hbar\omega-3E_j+2i\Gamma_j}{\left(\hbar\omega-E_j+i\Gamma_j\right)^2}-\frac{2\hbar\omega+3E_j+2i\Gamma_j}{\left(\hbar\omega+E_j+i\Gamma_j\right)^2}\right), \end{aligned} \tag{2.50}$$

where A$_j$=$(8\pi e^2\hbar^2A'_j)/(\mathrm{m}^2\mathrm{E}_j^2)$, B$_j$=$(3\alpha_j/2)A_j$.

Similarly, the expression of $\varepsilon(\omega)$ in the vicinity of critical points of types M_1, ..., M_3 by substitution of eqs. 2.36- 2.38 into eq. 2.34 can be obtained.

2.6 Conclusion

We had dealt with the mathematical representations that are employed to describe polarized light, and we used these representations to discuss the interaction of polarized light with the optical components that may compose an ellipsometer. The mathematical tool are applied to analyze the theory of measurement in ellipsometer, including to give a relation between the SE parameters (Δ and Ψ) and the normalized Fourier coefficients (a_2 and b_2) of the rotating-analyzer system. On the reflection of polarized light by stratified planner structures is intended to provide results and techniques that are essential for the interpretation of ellipsometric data in terms of the macroscopic properties of particular sample under measurement. We have also described the Levenberg-Marquardt Method, which was widely applied to analyze SE data.

We place emphasis on our proposed analysis model (Modified Harmonic Oscillator Approximation Scheme for the Dielectric Constants of Semiconductor). The model presented here is mathematically simple, and related to the electronic energy-band structures of the medium. This model is applicable over the entire range of photon energies, below and above the lowest band gaps, and it exactly satisfies the Kramers-Kronig relations. It also requires the minimum number of parameters to yield excellent simultaneous fits to $\varepsilon_1(\omega)$ and $\varepsilon_2(\omega)$ and their first three numerical derivatives with respect to photon energy.

References

[1] R. C. Jones, J. Opt. Soc. Am. **31** 488 (1941).

[2] E. L. O'Neill, Introduction to Statistical Optics (Addison-Wesley, Reading, Massachusetts, 1963). Ch. 9.

[3] B. D. Cahan and R. F. Spanier, Surf. Sci., **16**, 166 (1969).

[4] R. Greef, Rev. Sci. Instr. **41**, 532 (1970).

[5] P. S. Hauge and F. H. Dill, IBM J. Res. Dev. **17**, 472 (1973).

[6] D. E. Aspnes, J. Opt. Soc. Am., **64**, 812 (1974).

[7] D.E. Aspnes and A, A. Studna, Appl. Opt.., **14**, 220 (1975).

[8] C. Pickering, in Handbook of Crystal Growth Vol. III. D. J. T. Hurle, (Ed.), North-Holland, Amsterdam.

[9] D. E. Aspnes and A. A. Studna, Appl. Phys. Lett., **39**, 316 (1981).

[10] R. M. A. Azzam and N. M. Bashare, Ellipsometry and Polarized Light (North-Holland, Amsterdam, 1977).

[11] Fred L. Terry, Jr., J. Appl. Phys., **70**,409 (1991).

[12] W. H. .Press, B. P. Flannery, S. A. Teukolsky and W. T. Vetterling, Numerical Recipes: The Art of Scientific Computing (Cambridge University Press, Cambridge, England), 523ff.

[13] P. G. Snyder, M. C. Rost, G. H. Bu-Abbud, J. A. Woollam and S. A. Alterovitz, J. Appl. Phys., **60** 3293 (1986).

[14] C. Pickering, R. T. Carline, D. J. Robbine, W. Y. Leong, S. J. Barnett, A. D. Pitt and A. G. Gullis, J. Appl. Phys., **73**, 239 (1993).

[15] G. Yu, T. Soga, T. Jimbo and M. Umeno, Jpn. J. Appl. Phys., **34**, 530 (1995).

[16] P. Lautenschlager, M. Garriga, L. Vina and M. Cardona, Phys. Rev. B **36**, 4821 (1987).

[17] S. Zollner, M. Garriga, J. Humllcicek and M. Cardona, Thin Solid Films **233**, 185 (1993).

[18] M. Erman, J. B. Theeten and P. Frijink, J. Appl. Phys., **56**, 3241 (1984).

[19] M. Erman, J. B. Theeten and P. Chambon, J. Appl. Phys., **56**, 2664 (1984).

[20] F. L. Terry, Jr., J Appl. Phys., **70**, 409 (1991).

[21] C. C. Kim, J. W. Garland, H. Abad and P. M. Raccah, Phys. Rev. B **45**, 11 749 (1992).

[22] L. Van Hove, Phys. Rev. **89**, 1189 (1953).

[23] Handbook of Optical Constants of Solids, ed. E. D. Palik (Academic, New York, 1985).

[24] D. E. Aspnes and A. A. Studna, Phys. Rev. B **27**, 985 (1983).

[25] M. Erman, J. P. Andre and J. Lebris, J. Appl. Phys., **59**, 2019 (1986).

[26] M. Erman, J. B. Theeten, N. Vodjdani and Y. Demay, J. Vac. Sci. Technol. B **1**, 328 (1983).

[27] M. Cardona, Modulation Spectroscopy, Suppl. 11 of Solid State Physics (Academic, New York, 1969).

[28] D. E. Aspnes, in Handbook on Semiconductors, edited by M. Balkanski (North-Holland, Amsterdam, 1980), Vol. 2, p. 109.

[29] S. M. Kelso, D. E. Aspnes, M. A. Pollack and R. E. Nahory, Phys,Rev. B **26**, 6669 (1982).